Articles

Determinants of Retinoid X Receptor Transcriptional Antagonism

Claudio N. Cavasotto,[||] Gang Liu,[†] Sharon Y. James,[†] Peter D. Hobbs,[‡] Valerie J. Peterson,[#] Ananyo A. Bhattacharya,[†] Siva K. Kolluri,[†] Xiao-kun Zhang,[†] Mark Leid,[#] Ruben Abagyan,[§] Robert C. Liddington,[†] and Marcia I. Dawson*[,†]

Cancer Center, The Burnham Institute, 10901 North Torrey Pines Road, La Jolla, California 92037, Molsoft L.L.C., 3366 North Torrey Pines Court, Suite 300, La Jolla, California 92037, Retinoid Program, SRI International, 333 Ravenswood Avenue, Menlo Park, California 94025, College of Pharmacy, Oregon State University, Corvallis, Oregon 97331, and The Scripps Research Institute, 10550 North Torrey Pines Road, La Jolla, California 92037

Received December 31, 2003

The synthesis and bioactivity of the retinoid X receptor (RXR) antagonist 4-[(3′-*n*-butyl-5′,6′,7′,8′-tetrahydro-5′,5′,8′,8′-tetramethyl-2′-naphthalenyl)(cyclopropylidene)methyl]benzoic acid and several heteroatom-substituted analogues are described. Ligand design was based on the scaffold of the 3′-methyl RXR-selective agonist analogue and reports that 3′-*n*-propyl and longer *n*-alkyl groups conferred RXR antagonism. The transcriptional antagonism of the 3′-*n*-butyl analogue was demonstrated by its blockade of retinoic acid receptor (RAR) β expression induced by the RXRα/peroxisome proliferator-activated receptor (PPAR) γ heterodimer complexed with an RXRα agonist plus the PPARγ agonist ciglitazone and the inhibition of 9-*cis*-RA-induced coactivator SRC-1a recruitment to RXRα. Receptor−ligand docking studies using full-atom flexible ligand and flexible receptor suggested that binding of the antagonist to the RXRα antagonist conformation was favored because the salt bridge that formed between the retinoid carboxylate and the RXRα helix H5 arginine-321 was far stronger than that formed on its binding to the agonist conformation. The antagonist also blocked activation of RAR subtypes α and β by 9-*cis*-RA but not that of RARγ.

Introduction

The retinoid nuclear receptors function as transcription factors that regulate such cell processes as morphogenesis, proliferation, and differentiation.[1] This homologous retinoid receptor subfamily has two classes, namely, the retinoic acid receptors (RARs) and retinoid X receptors (RXRs). Each class consists of three subtypes (α, β, and γ). In vivo, these receptors typically function as heterodimers that bind to specific DNA sequences termed response elements (REs) and undergo conformational changes on binding retinoid transcriptional agonists to release corepressors and recruit coactivators. Binding by the latter facilitates the interactions necessary to engage the multiprotein machinery for gene transcription. X-ray crystallographic studies indicate that transcriptional agonist binding induces major shifts in the RAR ligand-binding domain (LBD) helices H3, H11, and H12 so that helix H3 and the activation function-2 (AF-2) region of helix H12 form a cleft with helix H4 on the RAR surface to which a coactivator binds.[2,3] In contrast, RAR transcriptional antagonists are unable to effect these same changes. Crystallography on RXRα−agonist complexes reveals that the terminus of the RXRα helix H12 is more mobile.[4−7] These differences are highlighted by the structure of the RXRα/peroxisome proliferator activated receptor (PPAR) γ heterodimer complex with both RXR agonist 9-*cis*-RA (**1** in Figure 1) and PPARγ transcriptional agonist rosiglitazone[5] and by the transcriptional activation activity of the RXRα/RARα heterodimer complex with both RXR transcriptional agonist SR11237[8] (**2**) and RAR antagonist AGN192870 (**14**).[6] This inherent flexibility in the RXRα helix H12 permits the functional variability exhibited by RXR as the heterodimeric partner of many other members of the nuclear receptor family.[7]

Synthetic receptor-selective retinoids facilitate mechanistic studies[9−12] because the natural retinoids lack specificity with *trans*-RA (**15**) activating all the RAR subtypes, **1** activating both RAR and RXR subtypes,[1] and both interconverting by isomerization.[9] RAR class and subtype-selective transcriptional agonists and antagonists have been reported,[9−12] as have RXR class-selective retinoids (rexinoids).[8,9,11−18] The extensive homology of the RXR subtype ligand-binding pocket (LBP) residues has as yet precluded the identification of RXR subtype-selective retinoids. To facilitate mechanistic studies, we undertook the identification of RXR-selective transcriptional antagonists, as have other groups.[19−22] Previously, the homology between the residues surrounding the RAR and RXR LBPs[1] led to our successful exploitation of the mirrored structural

* To whom correspondence should be addressed. Telephone: 1-858-646-3165. Fax: 1-858-646-3197. E-mail: mdawson@burnham.org.
[||] Molsoft L.L.C.
[†] The Burnham Institute.
[‡] SRI International.
[#] Oregon State University.
[§] The Scripps Research Institute.

10.1021/jm030651g CCC: $27.50
Published on Web 07/29/2004

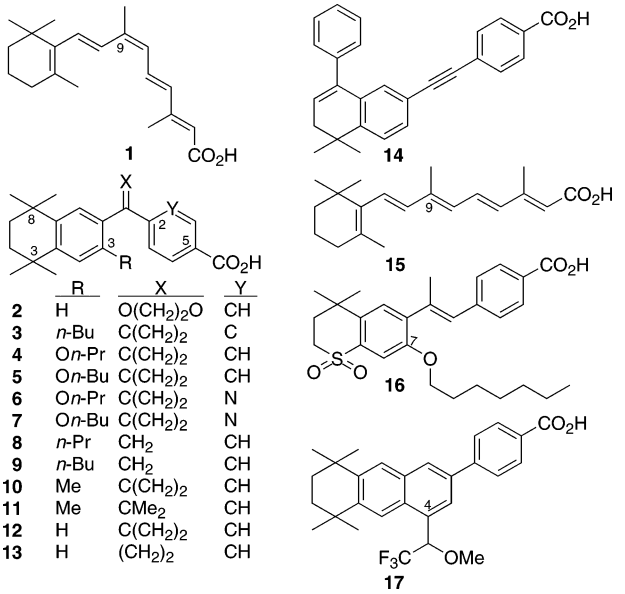

	R	X	Y
2	H	$O(CH_2)_2O$	CH
3	*n*-Bu	$C(CH_2)_2$	C
4	O*n*-Pr	$C(CH_2)_2$	CH
5	O*n*-Bu	$C(CH_2)_2$	CH
6	O*n*-Pr	$C(CH_2)_2$	N
7	O*n*-Bu	$C(CH_2)_2$	N
8	*n*-Pr	CH_2	CH
9	*n*-Bu	CH_2	CH
10	Me	$C(CH_2)_2$	CH
11	Me	CMe_2	CH
12	H	$C(CH_2)_2$	CH
13	H	$(CH_2)_2$	CH

Figure 1. Structures of RAR and RXR panagonist **1**, rexinoid agonists **2** and **8**−**13**, RXR antagonist **3** and analogues **4**−**7**, RAR antagonists **14** and **17**, RAR agonist *trans*-RA (**15**), and RARα-selective antagonist **16**.

similarities of their selective ligands to guide the design of RXR agonists based on that of RARγ agonists.[9,13,14] We then extended this strategy to RXR antagonist design from the structures of RAR antagonists. Here, we report one such RXR antagonist, 4-[(3′-*n*-butyl-5′,6′,7′,8′-tetrahydro-5′,5′,8′,8′-tetramethyl-2′-naphthalenyl)(cyclopropylidene)methyl]benzoic acid (**3**), and four heteroatom-substituted analogues, **4**−**7**.

To understand the structural determinants that govern receptor binding by **3**, we undertook computational studies on RAR and RXR ligand-binding domain (LBD)−retinoid complexes using state-of-the-art, full-atom flexible ligand−flexible receptor docking, a technique that we previously used successfully on G-protein-coupled seven-transmembrane receptors[23] and protein kinases.[24] The present studies suggested that the preference of retinoid **3** for the antagonist-bound conformation of the RXRα LBD[25] was not due to steric clashes with residues in the LBP of the agonist-bound conformation but to the greater strength of the salt bridge between the carboxylate group of **3** and the guanidinium group of arginine (R)-321 in helix H5 in the LBP of the antagonist-bound conformation. These studies provide evidence that ligand binding to these mobile retinoid receptors may be more complex than that anticipated from using rigid crystallographic structures as models.

Results

Earlier, retinoid **8**, which has a 3′-*n*-propyl group ortho to the ethenyl carbon joining its aryl rings, was reported to bind to the RXR subtypes but not to bind to the RAR subtypes or to activate the RAR or RXR subtypes.[16] Because this activity profile suggested that **8** was an RXR transcriptional antagonist, we synthesized its 3′-*n*-butyl analogue (**9**) as a potential antagonist for probing RXR-selective retinoid (rexinoid) signaling pathways. Unfortunately, because **9** activated RXRα on the $(TREpal^{1})_2$-*tk*-chloramphenicol acetyl transferase (CAT) reporter construct (Table 1), further design and synthesis were necessary. Our first objective in the present studies was to discern whether the addition of hydrophobic substituents at the 2-position of the ethenyl bridge of **9** would produce an RXR antagonist as a similar strategy did for the diazepinyl-bridged rexinoids reported by Kagechika and co-workers.[19] The validity of such an approach has since been supported by their recent report on the conversion of a series of potent 1,3-pyrimidine-5-carboxylic acid-terminated, MeN-bridged rexinoid agonists to antagonists by replacing the 3′-methyl groups on their 5′,6′,7′,8′-tetrahydro-2′-naphthalenyl rings with 3′-*n*-pentoxy and *n*-hexyloxy groups.[20] Klaus and co-workers first reported the use of a 3′-*n*-alkoxy (*n*-heptyloxy) substituent to confer retinoid antagonist activity in RARα-selective Ro41-5253 (**16**).[26] We substantiated the utility of this substitution strategy in the related RAR antagonist **17**.[27]

In the construction of **3**, the potent RXR-selective agonist 4-[(5′,6′,7′,8′-tetrahydro-5′,5′,8′,8′-tetramethyl-2′-naphthalenyl)(cyclopropylidene)methyl]benzoic acid (**10**)[14] was used as the scaffold and the 3′-*n*-butyl group of **9** was used to introduce antagonist activity. The synthesis of **3**, which is illustrated in Scheme 1, was also based on that of **10**. Serendipitously for the first phase of this work, the 6-(*n*-butyl)tetrahydronaphthalene **19** was available as a byproduct from the lithiation of the 6-bromotetrahydronaphthalene **18** using an *n*-butyllithium solution evidently containing appreciable unreacted *n*-butyl halide. Subsequently, **19** was directly prepared in much higher yield by lithiation of **18** followed by alkylation with excess *n*-butyl bromide. The overall yield for the five-step synthesis of **3** from **18** was 28%. Substitution of methyl(triphenyl)phosphonium bromide in the fourth step of Scheme 1 afforded **9**.

This series was extended with heteroatom-substituted analogues **4**−**7** for the following reasons. Replacing the 3′-alkyl group on the TTN ring with an alkoxy group has been shown to facilitate the synthesis of rexinoid analogues.[16,20] Pyridine and pyrimidinecarboxylic acid termini were reported to confer high-binding affinities to RXRs having an MeN or cyclopropyl C bridge.[16,20] In addition, according to the Lipinski rule of five,[28] the introduction of an H-bond acceptor group should improve druglike properties. Thus, the 3′-*n*-propoxy and 3′-*n*-butoxy-5′,6′,7′,8′-tetrahydro-5′,5′,8′,8′-tetramethyl-naphthalenyl (TTN) benzoic acid analogues **4** and **5** of

Table 1. Effects of Retinoids **3** and **9** on Retinoid Receptor Activity Induced by **1** on the TREpal Retinoid Response Element[a]

	relative activation (%)											
	RXRα concn (M)			RARα concn (M)			RARβ concn (M)			RARγ concn (M)		
	10^{-7}	10^{-6}	10^{-5}	10^{-7}	10^{-6}	10^{-5}	10^{-7}	10^{-6}	10^{-5}	10^{-7}	10^{-6}	10^{-5}
3	115 ± 5	88 ± 4	48 ± 4	82 ± 3	45 ± 3	22 ± 1	98 ± 4	88 ± 3	65 ± 3	95 ± 4	99 ± 3	91 ± 5
9	114 ± 4	130 ± 6	150 ± 11	75 ± 3	30 ± 2	20 ± 1	94 ± 3	102 ± 4	84 ± 5	89 ± 5	94 ± 4	110 ± 6

[a] Receptor activities were determined using the $(TREpal)_2$-*tk*-CAT reporter construct in cotransfected CV-1 cells as described[11] and expressed relative to that of 1×10^{-7} M **1** as 100%.

Scheme 1[a]

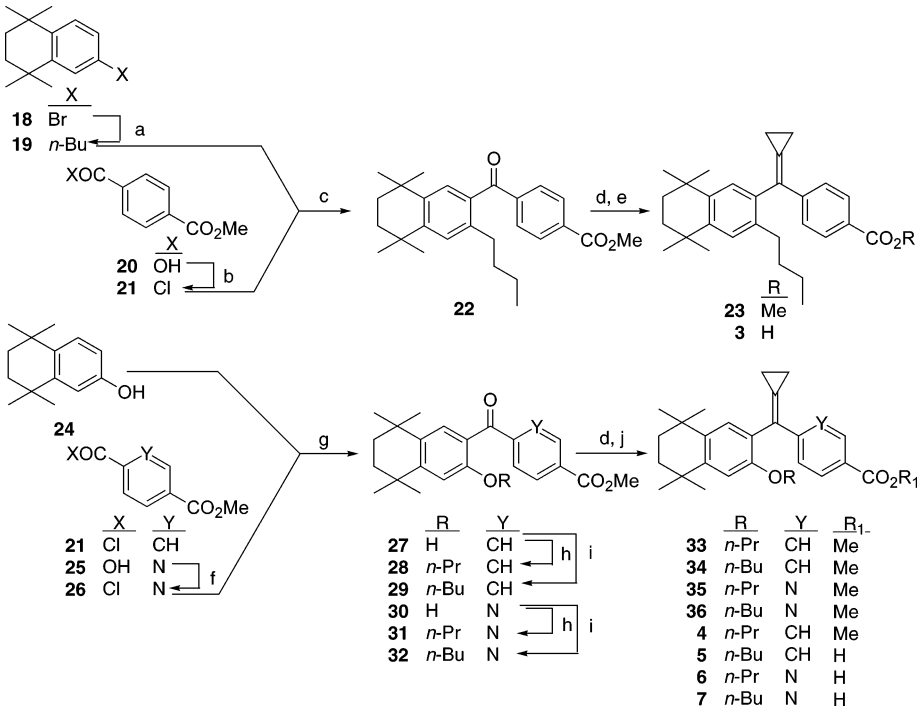

[a] (a) *n*-BuLi, THF; 20−35 °C, *n*-BuBr; (b) $(COCl)_2$, PhH, reflux; (c) $AlCl_3$, CH_2Cl_2, 0 °C to reflux; (d) [cyclopropylmethyl$(Ph)_3$PBr, $KN(SiMe_3)_2$, PhMe], $[Me(OCH_2CH_2)_2]_3N$, 100 °C; (e) aqueous KOH, EtOH, 80−90 °C, H_3O^+; (f) 5-carbomethoxypyridinecarboxylic acid (**25**), $SOCl_2$, DMF, benzene, reflux; (g) **21** or **26**, CH_2Cl_2, $AlCl_3$; (h) (**28** and **31**) *n*-PrBr, K_2CO_3, acetone, reflux; (i) (**29** and **32**) *n*-BuBr, K_2CO_3, acetone, reflux; (j) aqueous NaOH, MeOH, reflux; dilute HCl.

3, as well as their 5-pyridinecarboxylic acid analogues **6** and **7**, were readily prepared from the tetrahydrotetramethylnaphthol **24** and the benzoyl chloride **21** and the 2-pyridylcarbonyl chloride **26** by routes that were very similar to that used for the preparation of **3** (Scheme 1). However, in the cases of **4**−**7**, Fries rearrangements were used to introduce the aroyl groups of acyl chlorides **21** and **26** at the least hindered position adjacent to the OH group on **24** to produce **27** and **30**, respectively. Alkylation of the hydroxyl groups of **27** and **30**, Wittig olefination of the diaryl ketone group of the resulting aryl ethers **28**, **29**, **31**, and **32**, and methyl ester hydrolysis of the Wittig reaction products **33**−**36** then produced **4**−**7** in overall yields of 67%, 66%, 24%, and 25%, respectively, for the five steps starting from **24**.

Rexinoid 3 binds to RXRα. Competitive binding studies using recombinant histidine-tagged human (h) RXRα LBD and [11,12-$^3H_2$]9-*cis*-RA indicated that the relative binding affinities as measured by IC_{50} values were 21 nM for **10**, 29 nM for **1**, and 0.5 μM for **3** (Figure 2). Thus, under these conditions, **3** was a more than 20-fold weaker competitive binder to RXRα than the agonist **10** from which it was derived. Binding affinity assays using a second recombinant hRXRα LBD sample indicated that heteroatom substitution on the scaffold of **3** improved binding affinity to RXRα. Relative IC_{50} values for **4**−**7** were 120, 270, 6, and 10 nM, respectively, compared to 45 nM for **1**. Thus, on the basis of comparing the IC_{50} values of **4** with **5** and of **6** with **7**, CH_2 homologation of the 3′-propoxy group decreased binding affinity by about half. In contrast, the pyridine rings of **6** and **7** enhanced affinity at least an order of magnitude over that of **4** and **5** having benzene rings at the same position.

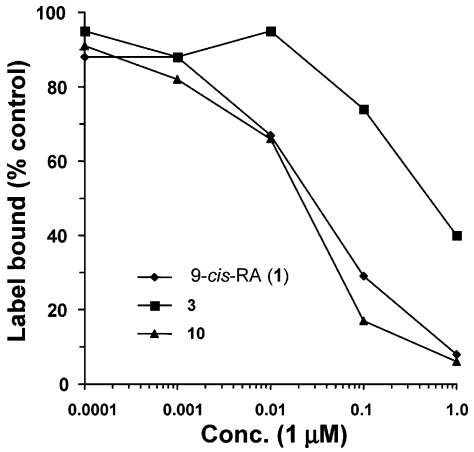

Figure 2. Binding affinity of **3** and **10** to the RXRα LBD. Competitive radioligand binding assays were performed as described in Methods. Binding was conducted in duplicate. Differences were 10% or less. The data represent the relative percentage of bound cpm compared to cpm bound in the absence of added ligand.

RXRα activation by 9-*cis*-RA (1) or rexinoid 2 is antagonized by 3. The retinoid receptor transcriptional activation activity of **3** was assessed in classical cotransfection assays. Transcriptional activation in CV-1 cells using cotransfected vectors for one of the retinoid receptors and a retinoid-responsive chloramphenicol acetyl transferase (CAT) reporter construct (the $(TREpal)_2$-*tk*-CAT,[1] RAR-specific cellular retinol-binding protein (CRBP)-I-*tk*-CAT,[1] or RXR-specific CRBP-II-*tk*-CAT[8]) showed that 1 μM **3** was not able to activate RARα, β, or γ or RXRα (Table 1). The TREpal is a palindromic response element that is activated by either RAR or RXR−agonist complexes. However, a 1 log

Table 2. Effects of Retinoid **3** on Retinoid Receptor Activity Induced by 9-*cis*-RA (**1**) on the CRBP-II and *trans*-RA (**15**) on the CRBP-I[a]

	relative activation (%)											
	RXRα concn (M)			RARα concn (M)			RARβ concn (M)			RARγ concn (M)		
	0	10^{-7}	10^{-6}	0	10^{-7}	10^{-6}	0	10^{-7}	10^{-6}	0	10^{-7}	10^{-6}
3	100	98 ± 6	34 ± 2	100	52 ± 4	10 ± 2	100	80 ± 4	59 ± 1	100	94 ± 8	108 ± 6

[a] RXRα and RAR subtype activities were determined using the CRBP-II-*tk*-CAT and CRBP-I-*tk*-CAT reporter constructs, respectively, in cotransfected CV-1 cells treated with 1×10^{-7} M 9-*cis*-RA and 1×10^{-7} M *trans*-RA, respectively, in the absence or presence of the indicated concentrations of **3** as described[121] and expressed relative to that of 1×10^{-7} M 9-*cis*-RA as 100% for RXRα activation and 1×10^{-7} M *trans*-RA as 100% for the RAR subtype activations.

excess of **3** was able to reduce 0.1 μM **1**-induced RXRα activation of the CRBP-II by over 66% (Table 2) and that induced by 0.1 μM rexinoid agonist **2** by 80%. Interestingly, antagonism by **3** was weaker on the $(TREpal)_2$-*tk*-CAT reporter because a 2 log excess of **3** was required to decrease **1**-induced RXRα activation by 50%. Thus, while having no intrinsic RAR subtype or RXRα agonist activity, **3** was able to successfully block the activation of RARα and RARβ by *trans*-RA (**15**) or **1** and that of RXRα by **1**. However, **3** had only minimal effects on the activation of RARγ by **15** or **1** (Table 2).

In contrast to the inhibitory effects of **3** on **1**-induced RXRα activation, at 0.1, 1.0, and 10 μM **9** enhanced the activation of RXRα by 10 nM **1** on the $(TREpal)_2$-*tk*-CAT reporter in a concentration-dependent manner (114%, 130%, and 150%, respectively) (Table 1). At 1.0 and 10 μM, **9** reduced RARα activation by 10 nM **1** to 30% and 20%, respectively. The inhibitory effects of 10 μM **9** on RARβ and RARγ activation were considerably smaller (reduction from 92% to 82% and none, respectively). On the basis of these results, **9** functioned as an RXRα transcriptional agonist and an RARα antagonist.

Activation of the RARβ$_2$ response element (β$_2$RARE) by RXRα/PPARγ heterodimer ligands is blocked by antagonist 3. RARβ is considered to function as a tumor suppressor gene for several reasons. The loss of RARβ expression in many cancer cell lines and in tumor biopsy specimens has been found to correlate with their insensitivity to growth inhibition by retinoid agonists.[29,30] Restoration of RARβ expression by activating the β$_2$RARE response element in the RARβ$_2$ gene promoter with transfected RARα in the presence of a retinoid agonist or by transfection of RARβ$_2$ also restored the sensitivity of several cancer cell lines to growth inhibition by retinoids.[31,32] Recently, we observed that the combination of rexinoid transcriptional agonist **2** and the PPARγ agonist ciglitazone cooperatively transactivated the transfected β$_2$RARE reporter construct in both retinoid-resistant MDA-MB-231 and retinoid-sensitive ZR-75-1 breast cancer cells.[33] Antagonist **3** was able to block the induction of RARβ protein expression in the Calu-6 lung cancer cell line by the combination of rexinoid **2** and ciglitazone (Figure 3).

Coactivator recruitment to RXRα is inhibited by antagonist 3. Retinoid transcriptional agonists induce conformational changes in the retinoid receptor LBD that permit coactivator binding, whereas antagonists do not. Unlike RXR agonist **1** and RXR-selective agonists **10**−**12**,[13,14] antagonist **3** was not able to induce the recruitment of the steroid receptor coactivator (SRC)-1a[34] to the RXRα LBD coactivator site in vitro but did retard the recruitment of SRC-1a induced by **1**, as was

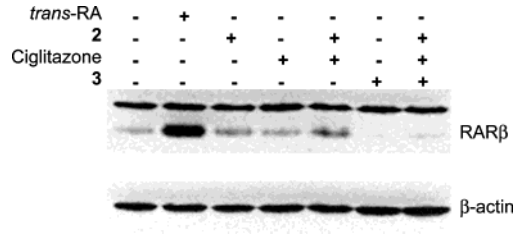

Figure 3. Retinoid **3** inhibits RARβ induction by rexinoid agonist **2** and the PPARγ ligand ciglitazone. Calu-6 cells were treated for 24 h with 1.0 μM *trans*-RA (**15**), **2**, or **3**, or with 10 μM ciglitazone alone, or with **2** plus ciglitazone in the absence or presence of **3**. Cell lysates were prepared, and RARβ protein was assessed by Western analysis.

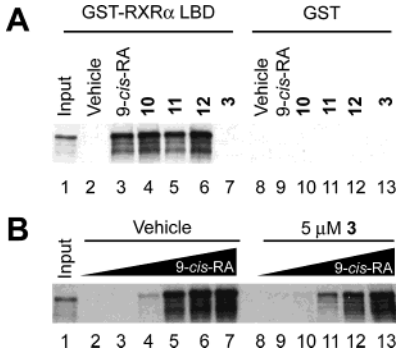

Figure 4. Antagonist **3** prevents coactivator recruitment to RXRα. (A) GST-pulldown experiments using GST-RXRα LBD or GST and [^{35}S]methionine-labeled, full-length SRC-1a (SRC-1) in the presence of vehicle (0.1% v/v ethanol, lanes 2 and 8) or RXR ligand as indicated. These experiments were conducted as previously described[34] with ligands at a final concentration of 1.0 μM. (B) GST-pulldown experiments as described in (A) using 1.0 μM **1** in the absence (lanes 2−7) or presence (lanes 8−13) of 5.0 μM **3**. The input lane (lane 2 of parts A and B) corresponds to 15% of the [^{35}S]methionine-labeled SRC-1a used in the pulldown reaction. The autoradiographs are representative of three independent experiments.

demonstrated in the glutathione-*S*-transferase (GST) pulldown experiments using the recombinant mouse RXRα LBD and ^{35}S-labeled SRC-1a that are shown in Figure 4. RXRα agonists **1** and **10**−**12** strongly promoted SRC-1a binding to the GST-RXRα LBD in vitro (Figure 4A, lanes 3−6). This result is consistent with the transcriptional activation properties of these ligands. In contrast, **3** did not promote SRC-1a interaction with the GST-RXRα LBD (Figure 4A, lane 7). The findings that **3** and **10**−**12** did not promote the interaction of SRC-1a with GST alone indicate the specificity of the interaction between the GST-RXRα LBD and SRC-1a (Figure 4A, lanes 9−13). This result and the demonstration that the binding of **3** and that of labeled 9-*cis*-RA to the RXRα LBD were mutually exclusive (Figure 2) suggested that **3** exerts RXRα antagonistic activity in

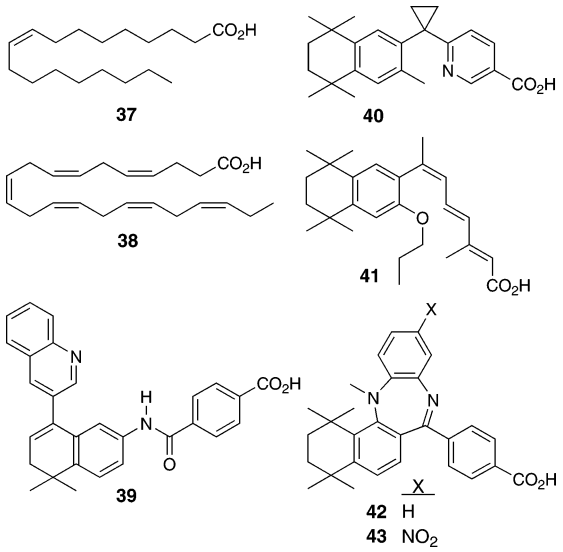

Figure 5. Structures of RXR antagonists **37**, **41**, and **43**; RXR transcriptional agonists **38**, **40**, and **42**; and RARα-selective antagonist **39**.

vitro. This possibility was tested directly in GST-pulldown assays, the results of which are shown in Figure 4B. When **3** was absent, **1** promoted receptor-SRC-1a interaction in a concentration-dependent manner (Figure 4B, lanes 3−7). In the presence of **3** at 5.0 μM, a concentration at which receptor−coactivator interaction did not occur (compare lanes 1 and 8 of Figure 4B), the efficacy with which **1** induced recruitment of SRC-1a to the RXRα LBD was clearly reduced (compare lanes 3−7 to lanes 9−13 in Figure 4B). However, because the **3**-mediated antagonism of **1**-induced recruitment of SRC-1a to the RXRα LBD was surmounted by increasing the concentration of **1** (compare lanes 7 and 13 in Figure 4B, which correspond to 1.0 μM **1**), **3** functioned as a competitive antagonist and not as a rexinoid agonist. Thus, binding by **3** to the RXRα LBD did not induce a conformation that could recruit a coactivator protein to the RXRα AF-2 site. Considered together, these in vitro studies demonstrated that **3** bound directly to the RXRα LBD but in a manner distinct from that of **1**.

Computational Studies. To understand how **3** functioned as a rexinoid antagonist in binding to the RXRα LBD, its docking conformation was compared to those of rexinoid agonists **10** and **13**,[13] which have C═C(CH$_2$)$_2$ and C(CH$_2$)$_2$ diaryl bridges, respectively. Docking studies were performed using the X-ray crystallographic structures of the RXRα LBDs complexed to **1** and 9-*cis*-oleic acid (**37** in Figure 5) to represent the agonist[35] (Protein Data Bank (PDB) entry 1FM6) and antagonist[2] (PDB 1DKF) conformations of the holo-RXRα LBD−retinoid complex, respectively. Water molecules in the vicinity of the ligand were taken from the PDB 1DKF structure for the antagonist conformation and the PDB 1FBY structure for the agonist conformation because no water molecules in the vicinity of the ligand were reported for the PDB 1FM6 structure. Rapid grid dockings with flexible ligands followed by global energy stochastic optimizations using the full-atom representations of the receptors and flexible ligands[36] were performed. Rexinoid agonists **10** and **13** had very good docking scores to the RXRα LBD agonist conformation, which were comparable to that of **1**. Superposing the docked configurations of **10** and **13** showed that their scaffold orientations were conserved (Figure 6A). Both **10** and **13** made similar contacts with the LBP surface, although those of **10** covered about 20% more of the surface. Both the higher contact surface and the slightly stronger electrostatic interaction between the carboxylate group of **10** and the guanidinium group of the RXRα LBD helix H5 arginine-316 (1FM6 numbering)[35] suggested why **10** had the lower IC$_{50}$ value in competitive binding to RXRα (21 nM for **10** compared to 44 nM for **13**) and a 2-fold lower AC$_{50}$ value for activating RXRα on the (TREpal)$_2$-*tk*-CAT than **13**.[14]

The docked conformation of **3** made considerable contacts with LBP residues in the RXRα LBD antagonist conformation. Its carboxylate group made a strong salt bridge with arginine-321 in helix H5 (1DKF numbering).[2] Surprisingly and despite our experimental studies demonstrating that **3** functioned as an RXRα antagonist (Table 1 and Figures 3 and 4), **3** was also able to dock to the RXRα LBD agonist conformation (Figure 6B). We next undertook docking experiments to assess whether the structural determinants for binding to the RXRα LBD antagonist conformation[2] were preferred by **3**. From the conformations we had generated by grid docking, we performed cycles of global energy stochastic optimization using both flexible ligand and flexible LBP side chains and then minimized the energy of resultant complexes. This full-atom flexible ligand−flexible receptor method revealed that in the agonist LBP conformation **3** superposed well with the native ligand **1** (Figure 6B). In this docking simulation, the two water molecules that were found in the vicinity of the ligand (RXRα LBD−**1**[35] PDB structure 1FBY) were conserved and were not affected by the benzoate group of **3**. One water molecule continued to hydrogen-bond to leucine-309, the carboxylate of **3**, and the second water molecule remained hydrogen-bonded to glutamine-275.

In the LBP antagonist conformation the TTN ring of **3** was rotated by 180° from that in the agonist conformation so that instead of the 3′-*n*-butyl group of **3** pointing to helix H11 in the LBP as it had in the agonist conformation, this group now pointed to helix H7. As a result, the benzoate group of **3** was nearly orthogonal (90°) to that in the agonist conformation and its carboxylate formed a strong salt bridge with the RXRα helix H5 arginine. During the course of this docking simulation, the water molecule that had originally hydrogen-bonded to the carbonyl oxygen of leucine-314 and the oleic acid (**37**) carboxylate in the LBP antagonist conformation was displaced from its position by the benzoate moiety of **3** and moved to become hydrogen-bonded to arginine-321, the hydroxyl hydrogen of serine-317, and the carboxylate of **3** (Figure 6C). Our calculations indicated that the salt bridge made by **3** in the antagonist conformation was much stronger than that in the agonist conformation. The binding affinity of **3** to the antagonist conformation was further strengthened by the reciprocal rearrangement of the LBP side chains that produced additional and closer hydrophobic contacts between **3** and the LBP surface than those produced in the agonist conformation (Figure 6D). Thus, these studies suggested that the binding of **3** to the

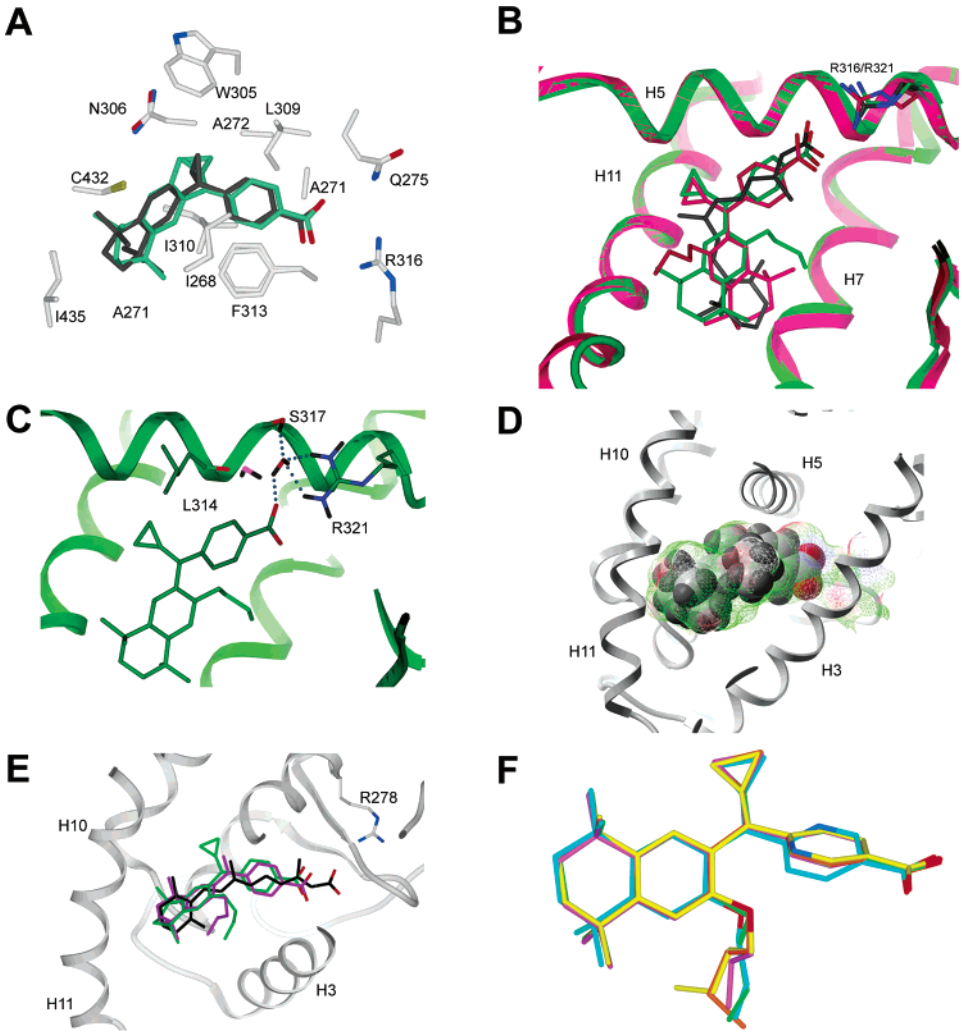

Figure 6. (A) Superposition of **10** (aqua) and **13** (dark-gray) in the human (h)RXRα ligand-binding pocket (LBP) after global optimization of side chains (carbon, gray; nitrogen, blue; oxygen, red; sulfur, yellow). (B) Superposition of complexes of **3** in the RXRα LBP in its agonist- (light-magenta) and antagonist-bound (green) conformations with that of **1** found in the agonist conformation. Some helices are indicated. The helix H5 arginine (R) 316 (agonist)/321 (antagonist) side chain conformations forming salt bridges with the ligand carboxylate conformations are also displayed. Retinoid **3** in the antagonist-bound conformation makes the stronger salt bridge with the RXRα LBD R321 and so functions as a competitive antagonist. The arginine nitrogens are in blue. (C) Hydrogen-bonding network of the water molecule making contacts with **3** (green) in the antagonist bound conformation of the RXRα LBP. The hydrogen bonds of the water contacting serine-317, arginine-321, and the carboxylate group of **3** are displayed in blue. This water as originally found hydrogen-bonded to leucine-314 and the **37** carboxylate (PDB 1DKF) is shown with its oxygen colored magenta. Atom color code: nitrogen, blue; oxygen, red; hydrogen, black. (D) Space-filling representation of **3** in the agonist-bound conformation of the hRARγ LBP indicating that **3** fits well (color coding of the pocket surface is green for hydrophobic regions, blue for hydrogen-bond donor, and red for hydrogen-bond acceptor). Helices H3, H5, H10, and H11 are indicated. (E) Superposition of **3** (green), **9** (purple), and *trans*-RA (**15**) (black) in the RARγ LBP shows the weaker electrostatic interaction for the carboxylate groups of rexinoids **3** and **9** with the helix H5 R278 side chain compared to that of *trans*-RA (**15**). R278 carbons are displayed in gray and nitrogens are in blue; ligand oxygens are in red. (F) Superposed conformations of **3**−**7** as found in docked to the RXRα LBD antagonist conformation. Structure color code: **3**, green; **4**, purple; **5**,; orange **6**, aqua; and **7**, yellow.

RXRα LBD antagonist conformation was energetically favored. We also performed flexible ligand−flexible receptor docking of analogues **4**−**7** to the antagonist conformation. As shown in Figure 6F, the high degree of overlapping of their resultant conformations with that of **3** suggested that the binding conformation of this series of ligands to the antagonist form of the RXRα LBD was conserved. Identical results were obtained performing the simulations in the absence of the water molecules.

Docking of **3** and **9** into the RARγ LBD agonist conformation using the structure of the human (h)RARγ LBD−*trans*-RA (**15**) complex[3] (PDB 2LBD) and the two water molecules reported to be in the vicinity of *trans*-RA (**15**) suggested that the lack of RARγ transcriptional activation activities for **3** and **9** was not due to any of their atoms clashing with those of RARγ LBP residues (Figure 6E). In fact, **3** and **9** fit very well in the LBP agonist conformation without any significant side chain clashes. Superposing the docked conformations of **3** and **9** with that of *trans*-RA (**15**)[3] (PDB entry 2LBD) revealed that electrostatic interactions between their retinoid carboxylates and the RARγ helix H5 arginine-278 were much weaker than those of *trans*-RA (**15**) (Figure 6E). As a result, the free energies[36] calculated for binding of **3** and **9** to the agonist form of the RARγ

LBD were about 4.5 kcal/mol higher than that for *trans*-RA (**15**). The same results were obtained when water molecules were omitted in the simulation. Thus, our computational studies agreed with experimental results on the lack of transcriptional activation of RARγ by **3** and **9**.

Discussion

The presence of clashes between a ligand and the side chains in the receptor LBP has been considered to be a prime determinant to its ability to bind. Our present docking studies suggest another paradigm in which the strength of the salt bridge formed between the retinoid carboxylate group and the guanidinium group of the conserved arginine on the RAR or RXR LBD helix H5 plays a major role in determining whether a retinoid functions as a transcriptional agonist or antagonist. Thus, **3** behaved as a transcriptional antagonist because the LBP side chain rearrangements that occurred on the binding of **3** to the RXRα LBP antagonist conformation produced a stronger salt bridge and more and closer hydrophobic contacts than those that occurred on its binding to the agonist conformation. The subtle difference in the energies of the resulting complexes would have shifted the equilibrium to favor the binding of **3** to the LBP antagonist conformation. Similarly, the stronger salt bridge between the carboxylate of rexinoid **10** and arginine-316 of the RXRα LBD agonist conformation and the resulting higher number of van der Waals contacts between **10** and the LBP surface would explain the higher binding affinity and transcriptional activation activity of **10** compared to **13**.[14] The results as to binding preferences to receptor agonist or antagonist conformations by these ligands remained the same regardless of whether the presence of water molecules in the vicinity of the salt bridge were included in the docking simulations.

The LBDs of the RARs and RXRs are flexible. X-ray crystallographic studies of the apo (nonliganded) and holo (liganded) RARγ and RXRα LBDs indicated that ligand binding produced significant and mutually cooperative conformational changes that influenced the position of their H12 helices. Thus, binding by a transcriptional agonist caused the N-terminus of the LBD helix H3 to tilt more than 10 Å and helix H11 to rotate 180° about its axis so that its hydrophobic side chains moved from the LBP to provide space for the ligand to bind. To accommodate the tilting of helix H3, helix H2 of RXRα unwound to increase the length of the loop between helices H1 and H3[35] and the loop joining helices H1 and H3 of RARγ straightened out. In agonist-bound RARs and RXRs, these changes allowed helix H12 to move to cap the LBP. In RARs, the position of the helix H12 was stabilized by direct interactions with the hydrophobic terminus of the ligand so that its AF-2 sequence formed the coactivator-binding site with helices H3 and H4.[35]

In RXRα, the position of the helix H12 C-terminus depended on the ligand bound, the dimeric partner, and whether a coactivator was present. Thus, in the RXRα LBD−**1**/PPARγ LBD−rosiglitazone−SRC-1 coactivator peptide complex, both the PPARγ and RXRα H12 AF-2 sequences formed coactivator-binding sites.[5] The RXRα LBD−RXR agonist **2**/RARα LBD−antagonist AGN192870 (**9**) complex also recruited a coactivator (TIF-II).[6] In the RXRα LBD−**1** monomer complex, the movement of helices H3 and H11 permitted stabilization of the hydrogen bonds between the N-terminus of helix H12 and helix H3 residues but not coactivator-binding site formation.[6] In contrast and unlike the binding of agonists to RARs, the agonists **1**, **2**, and docosahexaenoic acid (**38** in Figure 5) on binding to RXRα did not stabilize the RXRα helix H12 position through direct contacts.[7] In the RXRαF318A LBD mutant−oleic acid (**37**)/RARα LBD−RARα-selective antagonist BMS190614 (**39**) complex,[2] the H12 helices of both RXRα and RARα adopted comparable canonical antagonist conformations.[2] In this case, the RXRα helix H12 leucine-456, methionine-459, and leucine-460 side chains occupied the coactivator-binding site by mimicking the three leucines of the coactivator-binding motif. These studies indicate that the position of the RXR helix H12 varies considerably and is not stabilized by contacts with the ligand.

Moras and co-workers[35] reported that on docking the RXR agonist HX600 (**40**) into the LBP of the RXRα LBD−**1** complex the position of helix H12 was stabilized by van der Waals contacts with helices H5 and H11. In contrast, docking of the nitro-substituted analogue HX531 (**41**),[19] which functioned as an antagonist, produced steric clashes between the nitro group of **41** and helices H5 and H11. Docking of **41** to the RXRα LBD antagonist conformation[2] suggested to them that additional conformational adaptations of ligand or protein were required to ensure an acceptable fit.[35]

In the structure (1H9U)[37] for the RXRβ LBD homodimer complex with the potent rexinoid agonist 2-[1-(3′-methyl-5′,6′,7′,8′-tetrahydro-5′,5′,8′,8′-tetramethyl-2′-naphthalenyl)cyclopropyl]-5-pyridinecarboxylic acid (LG100268, **42**),[17] helix H12 by not contacting the receptor surface was found to have an apo, rather than a holo agonist, orientation. Love and co-workers speculated that had helix H12 assumed the classical agonist conformation on binding **42** and a coactivator, the 3′-methyl group on its TTN ring would have interacted with the RXRα leucine-451 to stabilize the helix H12 agonist conformation and coactivator interaction. They hypothesized that a longer 3′-group, such as the 3′-*n*-propoxy group of the RXR homodimer antagonist LG100754[22] (**43**), would have destabilized the helix H12 coactivator-binding site position through a similar interaction with helix H12.

Our docking studies do not support the latter premise but support the results of RXRα crystallographic studies by suggesting another binding paradigm. Docking results indicated that steric clashes of **3** with LBP residues of either helix H12 or other helices did not prevent docking to agonist conformations of the RXRα and RARγ LBDs. Instead, the binding of **3** to the agonist conformations of RXRα and RARγ was observed to be energetically disfavored. Antagonist **3** docked in the RXRα LBP antagonist conformation without significant steric clashes by adopting another configuration that enhanced the strength of its salt bridge to helix H5. Moreover, although docking of **3** to the RARγ LBD agonist conformation permitted salt bridge formation, the strength of this salt bridge was so much weaker than that formed by *trans*-RA (**15**) that efficient com-

petitive binding was not possible. These results suggest that ligand alignment in addition to steric clashing must be considered when conducting docking studies to retinoid receptors. Because a protein in solution exists in dynamic equilibrium with its environment and ligand, it is reasonable to assume that equilibration would favor the lowest-energy conformations of the receptor−ligand complex. Thus, in the case of the binding of **3** to RXRα, the antagonist conformation would predominate.

Methods

Chemistry. Materials. [11,12-$^3H_2$]9-*cis*-retinoic acid ([^{3}H]9-*cis*-RA, 43 Ci/mmol) was purchased (Amersham), and **1**,[38] SR11237 (**2**),[8] SR11173 (**10**),[14] SR11345 (**11**),[13] and SR11346 (**12**)[14] were synthesized as we described previously.

General. Unless otherwise mentioned, during workup procedures organic layers were washed with water and saturated brine, dried (anhydrous Na_2SO_4), filtered, and concentrated at reduced pressure. Standard column chromatography employed silica gel (Merck 60), as did flash chromatography (Merck, grade 9385, 230−400 mesh). Experimental procedures were not optimized and were typically conducted only once. Melting points were determined in sealed capillaries using a Mel-Temp II apparatus and are uncorrected. Fourier transform IR spectra were obtained on powdered samples, unless otherwise specified, using an FT-IR Mason satellite spectrophotometer. ^{1}H NMR spectra were recorded on a 300 MHz Varian Unity Inova spectrometer, and shift values are expressed in ppm (δ) relative to Me_4Si as the internal standard. Unless mentioned otherwise, compounds were dissolved in $^2HCCl_3$. MALDI-FTMS high-resolution mass spectra were run on an IonSpec Ultima instrument at The Scripps Research Institute (La Jolla, CA). Electrospray mass spectrometry was performed on an ABI EPI-3000 instrument.

6-*n*-Butyl-1,2,3,4-tetrahydro-1,1,4,4-tetramethylnaphthalene (19). To a stirred solution of 6-bromo-1,2,3,4-tetrahydro-1,1,4,4-tetramethylnaphthalene[13,39] (**18**) (1.34 g, 5.0 mmol) in THF (5 mL) under argon and cooled in a water bath was added a solution (3.0 mL) of 2.5 M *n*-BuLi (25 mmol) in hexanes dropwise to maintain the temperature between 20−35 °C. Stirring was continued for 1 h at room temperature. The reaction mixture was then cooled to −78 °C, and *n*-C_4H_9-Br (0.685 g, 5.0 mmol) in THF (2.0 mL) was added dropwise. This mixture was stirred at room temperature for 0.5 h before quenching with water and dilution with 1 N HCl and hexanes (100 mL). The organic layer was washed (brine, 3×), dried, and concentrated to give a pale-yellow liquid; TLC (hexanes) indicated one product (**19**, R_f = 0.66). Chromatography gave 1.01 g (83%) of **19** as a colorless liquid. IR ($CHCl_3$) 1466 cm^{-1}; ^{1}H NMR δ 0.94 (t, J = 7.2 Hz, 3H, 4′-CH_3), 1.28 (s, 12H, CH_3), 1.38 (m, 2H, 3′-CH_2), 1.58 (m, 2H, 2′-CH_2), 1.67 (s, 4H, 2,3-CH_2), 2.55 (d, J = 7.8 Hz, 2H, 1′-CH_2), 6.95 (d, J = 7.8 Hz, 1H, 7-ArH), 7.09 (s, 1H, 5-ArH), 7.20 ppm (d, J = 7.8 Hz, 1H, 8-ArH).

Methyl 4-(3′-*n*-Butyl-5′,6′,7′,8′-tetrahydro-5′,5′,8′,8′-tetramethyl-2′-naphthalenylcarbonyl)benzoate (22). To a suspension of 630 mg (3.5 mmol) of 4-carbomethoxybenzoic acid (**20**) in benzene (15 mL) was added oxalyl chloride (2.0 mL, 23 mmol). The mixture was heated at reflux for 2 h, cooled, and concentrated to give 4-carbomethoxybenzoyl chloride (**21**) as a white powder, which was used without further purification as follows. The powder was dissolved in CH_2Cl_2 (20 mL), and **19** (587 mg, 2.4 mmol) was added. This solution was cooled to 0 °C in an ice bath before $AlCl_3$ (1.06 g, 8 mmol) was added over a period of 15 min. After being stirred for 15 min at 0 °C, the mixture was heated at reflux for 0.5 h, poured into ice/water, and extracted with CH_2Cl_2 (100 mL). The combined organic layers were washed with water and brine, dried, and concentrated to give a yellow solid. Chromatography (2% EtOAc/hexane) afforded 820 mg (85%) of **22** as a white powder: mp 100−102 °C; TLC (5% EtOAc/hexane) R_f = 0.54; IR ($CHCl_3$) 1745 cm^{-1}; ^{1}H NMR δ 0.84 (t, J = 7.1 Hz, 3H, 4″-CH_3), 1.20 (s, 6H, CH_3), 1.30 (m, 2H, 3″-CH_2), 1.32 (s, 6H, CH_3), 1.50 (m, 2H, 2″-CH_2), 1.70 (s, 4H, 6′,7′-CH_2), 2.66 (t, J = 7.8 Hz, 2H, 1″-CH_2), 3.96 (s, 3H, OCH_3), 7.20 and 7.22 (2 s, 2H, 1′,4′-NapH), 7.86 (dd, J = 2.0, 6.6 Hz, 2H, 3,5-ArH), 8.11 ppm (dd, J = 1.9, 6.6 Hz, 2H, 2,6-ArH); MALDI-FTMS (HRMS) calcd $C_{27}H_{34}NaO_3$ (MNa^+) 429.2400, found 429.2412.

Methyl 4-[(3′-*n*-Butyl-5′,6′,7′,8′-tetrahydro-5′,5′,8′,8′-tetramethyl-2′-naphthalenyl)(cyclopropylidene)methyl]-benzoate (23). To a solution of cyclopropylmethyl(triphenyl)-phosphonium bromide (0.84 g, 2.2 mmol) dissolved in anhydrous toluene (2.0 mL) was added 0.5 M potassium bis(trimethylsilyl)amide (2.0 mmol) in toluene (4.0 mL) under argon at room temperature. Stirring was continued for 15 min before **22** (0.41 g, 1.0 mmol) and tris(2-methoxyethoxyethyl)amine (65 mg, 0.2 mmol) in toluene (1.5 mL) were added. The reaction mixture was heated in a 100 °C oil bath for 2 h to give a dark suspension, which was cooled, poured into aqueous $NaHCO_3$, and extracted (EtOAc). Drying and concentration gave a colorless oil, which was chromatographed (20−30% CH_2Cl_2/hexanes) to give 213 mg of three byproducts, then 173 mg of **23** (40%) as a white gum, followed by 144 mg (approximately 33%) of predominantly **23**. TLC (30% CH_2Cl_2/hexanes) R_f = 0.48; IR ($CHCl_3$) 1734, 1663 cm^{-1}; ^{1}H NMR δ 0.73 (t, J = 7.2 Hz, 3H, 4″-CH_3), 1.14 (m, 2H, 3″-CH_2), 1.25 (s, 6H, CH_3), 1.30 (m, 2H, 2″-CH_2), 1.33 (s, 6H, CH_3), 1.62 (m, 4H, C=C(CH_2)$_2$), 1.71 (s, 4H, 6′,7′-CH_2), 2.25 (t, J = 7.2 Hz, 2H, 1″-CH_2), 3.91 (s, 3H, OCH_3), 7.05 (s, 1H, 4′-NapH), 7.12 (s, 1H, 1′-NapH), 7.48 (d, J = 8.0 Hz, 2H, 3,5-ArH), 7.95 ppm (d, J = 8.4 Hz, 2H, 2,6-ArH); MALDI-FTMS (HRMS) calcd $C_{30}H_{39}O_2$ (MH^+) 431.2944, found 431.2939.

4-[(3′-*n*-Butyl-5′,6′,7′,8′-tetrahydro-5′,5′,8′,8′-tetramethyl-2′-naphthalenyl)(cyclopropylidene)methyl]benzoic Acid (3). Ester **23** (144 mg, 0.32 mmol) in EtOH (3.0 mL) and 20% KOH in water (1.0 mL) was heated at 80−90 °C for 2.0 h under argon, cooled to room temperature, and concentrated. The residue was acidified (1 N H_2SO_4), washed repeatedly (water), dried, and diluted (EtOAc/CH_2Cl_2) to give a cloudy suspension, which was eluted through a silica gel pad (1.5 cm × 20 cm) using 5% MeOH/CH_2Cl_2 (150 mL), then 0.25% HOAc/5% MeOH/CH_2Cl_2 to give 142 mg (100%) of **3** as a pale-yellow solid: mp 207−209 °C; TLC (50% EtOAc/hexane) R_f = 0.72; IR ($CHCl_3$) 2961, 1608 cm^{-1}; ^{1}H NMR (C^2HCl_3/MeOH-$^2H_4$) δ 0.73 (t, J = 7.3 Hz, 3H, 4″-CH_3), 1.15 (m, 2H, 3″-CH_2), 1.26 (s, 6H, CH_3), 1.30 (m, 2H, 2″-CH_2), 1.33 (s, 6H, CH_3), 1.63 (m, 4H, C=C(CH_2)$_2$), 1.71 (s, 4H, 6′,7′-CH_2), 2.25 (t, J = 7.0 Hz, 2H, 1″-CH_2), 7.05 (s, 1H, 4′-NapH), 7.13 (s, 1H, 1′-NapH), 7.52 (d, J = 8.5 Hz, 2H, 3,5-ArH), 8.02 ppm (d, J = 8.5 Hz, 2H, 2,6-ArH); MALDI-FTMS (HRMS) calcd $C_{29}H_{36}O_2$ (M^+) 416.2715, found 416.2715.

4-[1-(3′-*n*-Butyl-5′,6′,7′,8′-tetrahydro-5′,5′,8′,8′-tetramethyl-2′-naphthalenyl)ethenyl]benzoic Acid (9). To a solution of methyl(triphenyl)phosphonium bromide (0.79 g, 2.2 mmol) dissolved in anhydrous toluene (2.0 mL) was added 0.5 M potassium bis(trimethylsilyl)amide (2.0 mmol) in toluene (4.0 mL) under argon at room temperature. Stirring was continued for 15 min before **22** (0.41 g, 1.0 mmol) and tris(2-methoxyethoxyethyl)amine (65 mg, 0.2 mmol) in toluene (1.5 mL) were added. The reaction mixture was heated in a 100 °C oil bath for 2 h, then worked up and chromatographed as in the synthesis of ester **23** to give 148 mg (36%) of the ester of **9** as white crystals. TLC (30% CH_2Cl_2/hexanes) R_f = 0.42; ^{1}H NMR δ 0.76 (t, J = 7.3 Hz, 3H, 4″-CH_3), 1.17 (m, 2H, 3″-CH_2), 1.28 (s, 6H, CH_3), 1.31 (m, 2H, 2″-CH_2), 1.32 (s, 6H, CH_3), 1.71 (s, 4H, 6′,7′-CH_2), 2.25 (t, J = 8.0 Hz, 2H, 1″-CH_2), 3.91 (s, 3H, OCH_3), 5.31 (d, J = 1.4 Hz, 1H, C=CH), 5.81 (d, J = 1.4 Hz, 1H, C=CH), 7.09 and 7.10 (2 s, 2H, 1′,4′-NapH), 7.35 (dd, J = 1.5, 8.2 Hz, 2H, 3,5-ArH), 7.95 ppm (dd, J = 1.5, 8.1 Hz, 2H, 2,6-ArH).

The methyl ester of **9** (47 mg, 0.116 mmol) in EtOH (1.5 mL) and 20% aqueous KOH (0.5 mL) was heated at 80−90 °C for 2.0 h under argon, then cooled, concentrated, and diluted with 1.0 N H_2SO_4 to give a white solid that was thoroughly washed with water, then 10% EtOAc/hexanes. The resultant

solid was dissolved in 5% MeOH/$CHCl_3$, filtered, and concentrated to give after drying 42 mg (93%) of **9** as a white solid: mp 260−262 °C; TLC (50% EtOAc/hexanes) R_f = 0.70; IR ($CHCl_3$) 3416, 1663 cm^{-1}; ^1H NMR (C^2HCl_3/MeOH-$^2H_4$) δ 0.71 (t, J = 7.2 Hz, 3H, 4″-CH_3), 1.12 (q, J = 7.7 Hz, 2H, 3″-CH_2), 1.23 (s, 6H, CH_3), 1.27 (s, 6H, CH_3), 1.30 (m, 2H, 2″-CH_2), 1.66 (s, 4H, 6′,7′-CH_2), 2.22 (t, J = 7.5 Hz, 2H, 1″-CH_2), 5.21 (d, J = 1.4 Hz, 1H, C═CH), 5.72 (d, J = 1.4 Hz, 1H, C═CH), 7.05 (s, 2H, 1′,4′-NapH), 7.25 (d, J = 7.2 Hz, 2H, 3,5-ArH), 7.86 ppm (d, J = 8.7 Hz, 2H, 2,6-ArH); MALDI-FTMS (HRMS) calcd $C_{27}H_{35}O_2$ (MH^+) 391.2631, found 391.2616.

Tetrahydronaphthalene 24, Pyridinecarboxylate 25, and Benzoate 27. 5,6,7,8-Tetrahydro-5,5,8,8-tetramethyl-2-naphthol (**24**),[22] 5-carbomethoxypyridine-2-carboxylic acid (**25**),[40] and methyl 4-(5′,6′,7′,8′-tetrahydro-3′-hydroxy-5′,5′,8′,8′-tetramethyl-2′-naphthalenylcarbonyl)benzoate (**27**)[17] were synthesized according to the literature and had ^1H NMR spectra identical to those reported.

Methyl 2-(3′-Hydroxy-5′,6′,7′,8′-tetrahydro-5′,5′,8′,8′-tetramethyl-2′-naphthalenylcarbonyl)pyridine-5-carboxylate (30). To a suspension of 5-carbomethoxypyridine-2-carboxylic acid (**25**) (543 mg, 3.0 mmol) in benzene (5 mL) was added oxalyl chloride (1.0 mL, 11.5 mmol) and DMF (2 drops). This mixture was heated at reflux for 2 h, cooled, and concentrated to give 5-carbomethoxypyridine-2-carbonyl chloride (**26**) as a white powder, which was used without further purification in the next step.

The acyl chloride **26** dissolved in CH_2Cl_2 (20 mL) was added to a mixture of **24** (408 mg, 2.0 mmol) and $AlCl_3$ (1.33 g, 10 mmol) with cooling in an ice bath. After being stirred for 15 min at 0 °C, the reaction mixture was heated at reflux for 1 h. An additional portion of $AlCl_3$ (399 mg, 3.0 mmol) was added, and heating at reflux was continued for 0.5 h. The mixture was then cooled to room temperature, poured into ice/water, and extracted with CH_2Cl_2 (100 mL). The organic layers were washed (water and brine), dried, and concentrated to give a yellow solid, which on chromatography (5% EtOAc/hexane) afforded 380 mg (52%) of **30** as a golden powder: mp 162−164 °C; TLC (10% EtOAc/hexane) R_f = 0.32; IR ($CHCl_3$) 1730 cm^{-1}; ^1H NMR δ 1.16 (s, 6H, CH_3), 1.31 (s, 6H, CH_3), 1.68 (s, 4H, 6′,7′-H), 4.02 (s, 3H, OCH_3), 6.99 (s, 1H, 4′-NapH), 7.97 (d, J = 8.1 Hz, 1H, 3-PyH), 8.00 (s, 1H, 1′-NapH), 8.51 (dd, J = 2.1, 8.1 Hz, 1H, 4-PyH), 9.32 ppm (d, J = 1.8 Hz, 1H, 6-PyH). ESI-TOF (HRMS) calcd $C_{22}H_{26}NO_4$ (MH^+) 368.1862, found 368.1851.

General Method for the Synthesis of the *n*-Propyl and *n*-Butyl Ethers of Tetrahydronaphthols 27 and 30. To a solution of **27** or **30** (0.5 mmol) and *n*-propyl or *n*-butyl bromide (1.0 mmol) in acetone (10 mL) was added K_2CO_3 (4.0 mmol). The resulting suspension was heated at reflux for 20−24 h, at which time TLC showed that **27** or **30** had disappeared, then concentrated, and diluted with CH_2Cl_2 and water (20 mL each). The organic layer was washed (brine), dried, and concentrated. Chromatography (5% EtOAc/hexane) gave the *n*-propyl ether **28** (92%) or *n*-butyl ether **29** (93%) from **27** or the *n*-propyl ether **31** (84%) or *n*-butyl ether **32** (82%) from **30**.

Methyl 4-(3′-*n*-Propoxy-5′,6′,7′,8′-tetrahydro-5′,5′,8′,8′-tetramethyl-2′-naphthalenylcarbonyl)benzoate (28). White powder; mp 117−119 °C; TLC (4% EtOAc/hexane) R_f = 0.42; IR ($CHCl_3$) 1728 cm^{-1}; ^1H NMR δ 0.64 (t, J = 7.5 Hz, 3H, 3″-CH_3), 1.27 (s, 6H, CH_3), 1.32 (s, 6H, CH_3), 1.39 (m, 2H, 2″-CH_2), 1.71 (s, 4H, 6′,7′-H), 3.78 (t, J = 6.2 Hz, 2H, 1″-CH_2), 3.95 (s, 3H, OCH_3), 6.82 (s, 1H, 4′-NapH), 7.43 (s, 1H, 1′-NapH), 7.82 (d, J = 8.1 Hz, 2H, 3,5-ArH), 8.07 ppm (d, J = 8.1 Hz, 2H, 2,6-ArH); MALDI-FTMS (HRMS) calcd $C_{26}H_{33}O_4$ (MH^+) 409.2373, found 409.2359.

Methyl 4-(3′-*n*-Butoxy-5′,6′,7′,8′-tetrahydro-5′,5′,8′,8′-tetramethyl-2′-naphthalenylcarbonyl)benzoate (29). White powder; mp 96−97 °C; TLC (4% EtOAc/hexane) R_f = 0.43; IR ($CHCl_3$) 1728 cm^{-1}; ^1H NMR δ 0.64 (t, J = 7.5 Hz, 3H, 4″-CH_3), 1.00 (m, 2H, 3″-CH_2), 1.27 (s, 6H, CH_3), 1.31 (m, 2H, 2″-CH_2), 1.32 (s, 6H, CH_3), 1.70 (d, J = 1.2 Hz, 4H, 6′,7′-H), 3.81 (t, J = 6.6 Hz, 2H, 1″-CH_2), 3.95 (s, 3H, OCH_3), 6.81 (s, 1H, 4′-NapH), 7.43 (s, 1H, 1′-NapH), 7.81 (dd, J = 2.1, 6.6 Hz, 2H, 3,5-ArH), 8.07 ppm (dd, J = 1.8, 8.1 Hz, 2H, 2,6-ArH); MALDI-FTMS (HRMS) calcd $C_{27}H_{35}O_4$ (MH^+) 423.2530, found 423.2512.

Methyl 2-(3′-Propoxy-5′,6′,7′,8′-tetrahydro-5′,5′,8′,8′-tetramethyl-2′-naphthalenylcarbonyl)-5-pyridinecarboxylate (31). White powder; mp 135−137 °C; TLC (10% EtOAc/hexane) R_f = 0.28; IR ($CHCl_3$) 1728 cm^{-1}; ^1H NMR δ 0.59 (t, J = 7.5 Hz, 3H, 3″-CH_3), 1.26 (m, 2H, 2″-CH_2), 1.30 (s, 12H, CH_3), 1.69 (s, 4H, 6′,7′-H), 3.72 (t, J = 6.6 Hz, 2H, 1″-CH_2), 3.98 (s, 3H, OCH_3), 6.79 (s, 1H, 4′-NapH), 7.66 (s, 1H, 1′-NapH), 7.77 (d, J = 8.1 Hz, 1H, 3-PyH), 8.42 (dd, J = 2.4, 7.8 Hz, 1H, 4-PyH), 9.21 ppm (d, J = 2.1 Hz, 1H, 6-PyH); MALDI-FTMS (HRMS) calcd $C_{25}H_{32}NO_4$ (MH^+) 410.2326, found 410.2317.

Methyl 2-(3′-Butoxy-5′,6′,7′,8′-tetrahydro-5′,5′,8′,8′-tetramethyl-2′-naphthalenylcarbonyl)-5-pyridinecarboxylate (32). White powder; mp 115−117 °C; TLC (10% EtOAc/hexane) R_f = 0.28; IR ($CHCl_3$) 1733 cm^{-1}; ^1H NMR δ 0.70 (t, J = 7.2 Hz, 3H, 4″-CH_3), 0.93 (m, 2H, 3″-CH_2), 1.26 (m, 2H, 2″-CH_2), 1.30 (s, 12H, CH_3), 1.69 (s, 4H, 6′,7′-H), 3.75 (t, J = 6.3 Hz, 2H, 1″-CH_2), 3.98 (s, 3H, OCH_3), 6.78 (s, 1H, 4′-NapH), 7.66 (s, 1H, 1′-NapH), 7.86 (d, J = 8.1 Hz, 1H, 3-PyH), 8.43 (dd, J = 1.8, 8.4 Hz, 1H, 4-PyH), 9.21 ppm (d, J = 1.8 Hz, 1H, 6-PyH); MALDI-FTMS (HRMS) calcd $C_{26}H_{34}NO_4$ (MH^+) 424.2482, found 424.2461.

General Procedure for Introducing the (Cyclopropylidene)methyl Group into 28, 29, 31, and 32. To a solution of cyclopropylmethyl(triphenyl)phosphonium bromide (192 mg, 0.5 mmol) dissolved in anhydrous toluene (1.0 mL) was added 0.5 M potassium bis(trimethylsilyl)amide (0.5 mmol) in toluene (1.0 mL) under argon at room temperature. Stirring was continued for 1 h before diaryl ketone **28**, **29**, **31**, or **32** (0.2 mmol) and tris(2-methoxyethoxyethyl)amine (13 mg, 0.4 mmol) in toluene (0.5 mL) were added. The reaction mixture was stirred at room temperature for 1 h, then heated in a 100 °C oil bath for 2 h to give a dark suspension, which after cooling was poured into aqueous $NaHCO_3$ and extracted (EtOAc). Drying and concentration gave an oil, which was chromatographed (20−30% CH_2Cl_2/hexanes) to give the methyl ester **33** (87%), **34** (89%), **35** (62%), or **36** (67%), respectively.

Methyl 4-[(3′-*n*-Propoxy-5′,6′,7′,8′-tetrahydro-5′,5′,8′,8′-tetramethyl-2′-naphthalenyl)(cyclopropylidene)methyl]-benzoate (33). White gum; TLC (4% EtOAc/hexane) R_f = 0.57; IR ($CHCl_3$) 1723 cm^{-1}; ^1H NMR δ 0.60 (t, J = 7.5 Hz, 3H, 3″-CH_3), 1.26 (s, 6H, CH_3), 1.30 (m, 4H, 2″-CH_2, cyclopropyl H), 1.31 (s, 6H, CH_3), 1.54 (t, J = 7.8 Hz, 2H, cyclopropyl H), 1.70 (s, 4H, 6′,7′-H), 3.70 (t, J = 6.3 Hz, 2H, 1″-CH_2), 3.90 (s, 3H, OCH_3), 6.77 (s, 1H, 4′-NapH), 7.19 (s, 1H, 1′-NapH), 7.50 (d, J = 8.4 Hz, 2H, 3,5-ArH), 7.94 ppm (d, J = 8.4 Hz, 2H, 2,6-ArH).

Methyl 4-[(3′-*n*-Butoxy-5′,6′,7′,8′-tetrahydro-5′,5′,8′,8′-tetramethyl-2′-naphthalenyl)(cyclopropylidene)methyl]-benzoate (34). White gum; TLC (4% EtOAc/hexane) R_f = 0.58; IR ($CHCl_3$) 1725 cm^{-1}; ^1H NMR δ 0.70 (t, J = 7.5 Hz, 3H, 4″-CH_3), 0.97 (m, 2H, 3″-CH_2), 1.26 (s, 6H, CH_3), 1.28 (m, 4H, 2″-CH_2, cyclopropyl H), 1.31 (s, 6H, CH_3), 1.57 (t, J = 7.8 Hz, 2H, cyclopropyl H), 1.70 (s, 4H, 6′,7′-H), 3.73 (t, J = 6.3 Hz, 2H, 1″-CH_2), 3.90 (s, 3H, OCH_3), 6.76 (s, 1H, 4′-NapH), 7.20 (s, 1H, 1′-NapH), 7.48 (d, J = 8.4 Hz, 2H, 3,5-ArH), 7.93 ppm (d, J = 8.7 Hz, 2H, 2,6-ArH).

Methyl 2-[(3′-*n*-Propoxy-5′,6′,7′,8′-tetrahydro-5′,5′,8′,8′-tetramethyl-2′-naphthalenyl)(cyclopropylidene)methyl]-5-pyridinecarboxylate (35). White gum; TLC (10% EtOAc/hexane) R_f = 0.41; IR ($CHCl_3$) 1723 cm^{-1}; ^1H NMR δ 0.59 (t, J = 7.5 Hz, 3H, 3″-CH_3), 1.26 (m, 2H, 2″-CH_2), 1.28 (s, 6H, CH_3), 1.30 (s, 6H, CH_3), 1.40 (m, 2H, cyclopropyl H), 1.61 (m, 2H, cyclopropyl H), 1.69 (s, 4H, 6′,7′-H), 3.68 (t, J = 6.6 Hz, 2H, 1″-CH_2), 3.94 (s, 3H, OCH_3), 6.75 (s, 1H, 4′-NapH), 7.34 (s, 1H, 1′-NapH), 7.58 (d, J = 8.4 Hz, 1H, 3-PyH), 8.20 (dd, J = 2.4, 8.1 Hz, 1H, 4-PyH), 9.16 ppm (d, J = 2.1 Hz, 1H, 6-PyH).

Methyl 2-[(3′-*n*-Butoxy-5′,6′,7′,8′-tetrahydro-5′,5′,8′,8′-tetramethyl-2′-naphthalenyl)(cyclopropylidene)methyl]-5-pyridinecarboxylate (36). White gum; TLC (10% EtOAc/hexane) R_f = 0.42; IR ($CHCl_3$) 1726 cm^{-1}; ^1H NMR δ 0.59 (t, J = 7.5 Hz, 3H, 4″-CH_3), 0.94 (m, 2H, 3″-CH_2), 1.20 (m, 2H, 2″-

CH_2), 1.28 (s, 6H, CH_3), 1.30 (s, 6H, CH_3), 1.41 (m, 2H, cyclopropyl H), 1.57 (m, 2H, cyclopropyl H), 1.69 (s, 4H, 6′,7′-H), 3.68 (t, J = 6.6 Hz, 2H, 1″-CH_2), 3.94 (s, 3H, OCH_3), 6.74 (s, 1H, 4′-NapH), 7.35 (s, 1H, 1′-NapH), 7.57 (d, J = 8.4 Hz, 1H, 3-PyH), 8.21 (dd, J = 2.1, 8.4 Hz, 1H, 4-PyH), 9.15 ppm (d, J = 2.4 Hz, 1H, 6-PyH).

General Procedure for the Hydrolysis of Methyl Esters 33−36. Each ester (0.1 mmol) in MeOH (2.0 mL) and 10% aqueous NaOH (0.5 mL) was heated at 80−90 °C for 2.0 h under argon, cooled to room temperature, then diluted with EtOAc or CH_2Cl_2 (20 mL). The mixture was acidified (0.5 N HCl) and washed repeatedly (water and brine), then dried and concentrated to give the benzoic acid **4** (99%) or **5** (94%) or the pyridinecarboxylic acid **6** (89%) or **7** (88%).

4-[(3′-*n*-Propoxy-5′,6′,7′,8′-tetrahydro-5′,5′,8′,8′-tetramethyl-2′-naphthalenyl)(cyclopropylidene)methyl]-benzoic Acid (4). White powder; mp 226−228 °C; TLC (20% EtOAc/hexane) R_f = 0.34; IR ($CHCl_3$) 3405, 1728, 1689 cm^{-1}; ^1H NMR δ 0.60 (t, J = 7.5 Hz, 3H, 3″-CH_3), 1.26 (s, 6H, CH_3), 1.29 (m, 4H, 2″-CH_2, cyclopropyl H), 1.32 (s, 6H, CH_3), 1.58 (t, J = 7.8 Hz, 2H, cyclopropyl H), 1.70 (s, 4H, 6′,7′-H), 3.71 (t, J = 6.3 Hz, 2H, 1″-CH_2), 6.77 (s, 1H, 4′-NapH), 7.20 (s, 1H, 1′-NapH), 7.52 (d, J = 8.7 Hz, 2H, 3,5-ArH), 8.00 ppm (d, J = 8.1 Hz, 2H, 2,6-ArH). ESI-TOF (HRMS) calcd $C_{28}H_{35}O_3$ (MH^+) 419.2581, found 419.2572.

4-[1-(3′-*n*-Butoxy-5′,6′,7′,8′-tetrahydro-5′,5′,8′,8′-tetramethyl-2′-naphthalenyl)(cyclopropylidene)methyl]-benzoic Acid (5). White powder; mp 220−222 °C; TLC (20% EtOAc/hexane) R_f = 0.34; IR ($CHCl_3$) 3400, 1685 cm^{-1}; ^1H NMR δ 0.60 (t, J = 7.5 Hz, 3H, 4″-CH_3), 0.97 (m, 2H, 3″-CH_2), 1.27 (s, 6H, CH_3), 1.29 (m, 4H, 2″-CH_2, cyclopropyl H), 1.32 (s, 6H, CH_3), 1.58 (t, J = 9.0 Hz, 2H, cyclopropyl H), 1.70 (s, 4H, 6′,7′-H), 3.74 (t, J = 6.0 Hz, 2H, 1″-CH_2), 6.77 (s, 1H, 4′-NapH), 7.21 (s, 1H, 1′-NapH), 7.52 (d, J = 8.1 Hz, 2H, 3,5-ArH), 8.00 ppm (d, J = 7.8 Hz, 2H, 2,6-ArH). ESI-TOF (HRMS) calcd $C_{29}H_{37}O_3$ (MH^+) 433.2737, found 433.2724.

2-[(3′-*n*-Propoxy-5′,6′,7′,8′-tetrahydro-5′,5′,8′,8′-tetramethyl-2′-naphthalenyl)(cyclopropylidene)methyl]-5-pyridinecarboxylic Acid (6). White powder; mp 126−128 °C; TLC (50% EtOAc/hexane) R_f = 0.25; IR ($CHCl_3$) 3405, 1722 cm^{-1}; ^1H NMR δ 0.59 (t, J = 7.5 Hz, 3H, 3″-CH_3), 1.24 (m, 2H, 2″-CH_2), 1.28 (s, 6H, CH_3), 1.30 (s, 6H, CH_3), 1.40 (m, 2H, cyclopropyl H), 1.60 (m, 2H, cyclopropyl H), 1.69 (s, 4H, 6′,7′-H), 3.68 (t, J = 6.6 Hz, 2H, 1″-CH_2), 6.75 (s, 1H, 4′-NapH), 7.34 (s, 1H, 1′-NapH), 7.59 (d, J = 8.4 Hz, 1H, 3-PyH), 8.25 (dd, J = 1.8, 8.7 Hz, 1H, 4-PyH), 9.22 ppm (s, 1H, 6-PyH); MALDI-FTMS (HRMS) calcd $C_{27}H_{34}NO_3$ (MH^+) 420.2533, found 420.2528.

2-[(3′-*n*-Butoxy-5′,6′,7′,8′-tetrahydro-5′,5′,8′,8′-tetramethyl-2′-naphthalenyl)(cyclopropylidenyl)methyl]-5-pyridinecarboxylic Acid (7). White powder; mp 120−122 °C; TLC (50% EtOAc/hexane) R_f = 0.25; IR ($CHCl_3$) 3400, 1728 cm^{-1}; ^1H NMR δ 0.59 (t, J = 7.5 Hz, 3H, 4″-CH_3), 0.92 (m, 2H, 3″-CH_2), 1.21 (m, 2H, 2″-CH_2), 1.28 (s, 6H, CH_3), 1.30 (s, 6H, CH_3), 1.40 (m, 2H, cyclopropyl H), 1.60 (m, 2H, cyclopropyl H), 1.68 (s, 4H, 6′,7′-H), 3.72 (t, J = 6.0 Hz, 2H, 1″-CH_2), 6.74 (s, 1H, 4′-NapH), 7.35 (s, 1H, 1′-NapH), 7.61 (d, J = 8.1 Hz, 1H, 3-PyH), 8.27 (d, J = 7.8 Hz, 1H, 4-PyH), 9.23 ppm (s, 1H, 6-PyH); MALDI-FTMS (HRMS) cald $C_{28}H_{36}NO_3$ (MH^+) 434.2690, found 434.2670.

Receptor Model Construction. The agonist-bound human (h) RXRα LBD model was based on the X-ray crystal structure of the LBD bound to **1** at 2.1 Å resolution[5] (PDB entry 1FM6, chain A), which we selected on the basis of its high resolution and structural integrity. Because no water molecules were observed in the vicinity of the ligand in PDB 1FM6, the positions of water molecules in the vicinity of **1** were taken from those found in the LBP of the RXRα LBD−9-*cis*-RA complex in the PDB entry 1FBY structure.[35] The antagonist-bound hRXRα LBD model was derived from the crystal structure of the mouse RXRα LBD−F318A mutant bound to 9-*cis*-oleic acid (**37**) at 2.5 Å resolution[2] (PDB entry 1DKF, chain A) by virtually mutating the alanine at 318 back to the wild-type phenylalanine and then energy-minimizing the resulting structure in the internal coordinate space of the LBP that was within a 4.0 Å vicinity using the ICM method.[36,41,42] One water molecule in the vicinity of 9-*cis*-oleic acid (**37**) was kept in the simulations. The agonist-bound hRARγ LBD conformation was based on the X-ray structure reported for the *trans*-RA (**15**) bound complex[3] (PDB entry 2LBD, 2.0 Å resolution). Two water molecules in the vicinity of the native ligand carboxylate were kept in these simulations. As implemented in the ICM program, the PDB structures were adjusted by adding hydrogens and missing heavy atoms, assigning partial charges, and then energy-minimizing.

Energy Evaluation and Optimization. According to the ICM method, the molecular system was described using internal coordinates as variables. Energy calculations were based on the ECEPP/3[43] force field with a distance-dependent dielectric constant. The biased probability Monte Carlo[41,44] (BPMC) was used to optimize global energy by iterative cycles of a random conformational change of the free variables according to a predefined continuous probability distribution,[41,44] the local energy minimization of analytical differentiable terms, a complete energy evaluation including nondifferentiable terms such us entropy[41] and solvation energy, and the acceptance or rejection of the total energy on the basis of the Metropolis criterion.[45] The nonpolar contribution to the solvation energy in the implicit solvation model used was assumed to be proportional to the solvent-accessible surface, and the electrostatic contribution to solvation was determined from the Poisson equation using the boundary element algorithm.[46]

Ligand−Receptor Docking. In the flexible-ligand−rigid-receptor docking, the receptor was represented by six potential energy maps, namely, electrostatic, hydrogen bond, hydrophobic, and three van der Waals. The flexible ligand in the receptor field was subjected to global optimization[47] so that both the intramolecular ligand energy and the ligand−receptor interaction energy were optimized during the calculation. Each docked compound was assigned a score according to its fit in the LBP that also accounted for desolvation and hydrophobic effects and entropy loss, which occurred on docking.[24,47,48] Further structural refinement through flexible-ligand−flexible-receptor docking was achieved through cycles of global energy stochastic optimization[47,49] of the flexible ligand and flexible side chains within 6.0 Å of the ligand, followed by energy minimization of the complex, including backbone relaxations, which were important for relieving any residual van der Waals clashes between ligand and receptor. For the energy minimization of the complex, heavy atoms were tethered using quadratic restraints,[42] and the weight of the tether function was decreased after each minimization as follows: 50, 20, 10, 5, 1, and 0 kcal/mol.

Binding-Energy Calculations. The binding free energy calculation implemented in ICM[50] included an electrostatic term for Coulombic interactions and partial charge desolvation, a hydrophobic term for variation of the water/nonwater interface upon ligand binding, and an entropy term for loss of torsional entropy upon binding. A constant term for loss of translational/rotational entropy and change in entropy from variations in the concentration of free molecules was also included. No van der Waals term was used because it was considered too sensitive to small geometrical errors, whereas the average van der Waals interaction was included in the hydrophobic term because it was proportional to the surface interaction. No clashes between the ligand and the LBP were assumed in these calculations.

Biology. RXRα LBD Expression. A reported procedure[35] was modified. The cDNA sequence coding for the hRXRα LBD (amino acids 223−462) was amplified using the polymerase chain reaction (PCR) on forward 5′-AGTCCATATGACCAG-CAGCGCCAACGAG-3′ and reverse 5′-GCCGCTCGAGCT-AAGTCATTTGGTGCGG-3′ primers. The PCR product was purified (Gene Clean II kit, Q-Biogene) and then cloned into the vector pET15b (Novagen) using the NdeI and XhoI (New England Biolabs) restriction sites. After sequence conformation, the vector bearing the sequence for an N-terminus

hexahistidine tag was transformed into *E. coli* BL21 (DE3) (Novagen) for protein overexpression, for which a representative procedure is described. Cells were grown in TB medium containing bactotryptone, yeast extract, and glycerol in potassium phosphate (KP) buffer at 37 °C to an OD_{600} of 0.4−0.6, induced for 1−2 h with 0.25 mM 1-thio-β-D-galactopyranoside (Invitrogen), and then harvested by centrifugation. The cell pellet from 833 mL of culture was resuspended in 30 mL of buffer (5 mM imidazole, 500 mM NaCl, 20 mM Tris-HCl, pH 7.9), then stored at −80 °C until required. Upon thawing, the suspension was made 1 mM in 4-(2-aminoethyl)benzenesulfonylfluoride hydrochloride (Calbiochem) and sonicated on ice. The lysate was centrifuged (39000*g* for 30 min) to remove debris and purified on a 5-mL HiTrap Ni(II)-chelating column (Pharmacia Biotech) by sequentially washing (30 mL of 60 mM imidazole in 20 mM Tris-HCl, pH 7.9, containing 500 mM NaCl) and then eluting (30 mL of 100 mM EDTA in the same buffer). The His tag from the fusion protein was removed by proteolysis using thrombin. The hRXRα LBD (residues 223−462 plus the glycine−serine−histidine−methionine (GSHM) sequence remaining after cleavage of the His tag) was thoroughly dialyzed against 20 mM KP buffer, pH 7.9, containing 200 mM NaCl and analyzed by sodium dodecyl sulfate−polyacrylamide (SDS−PAGE) gel electrophoresis. A typical yield was 40 mg of RXRα LBD. Electrospray MS (GSHM + hRXRα LBD residues 223−462) calcd 27235.5, found 27234.8. The thrombin cleavage step was omitted for the protein used in competition binding assays.

Hexahistidine-tagged mouse RXRα lacking the AB domain (mRXRαΔAB) for the GST-pulldown experiments was expressed and purified as previously described.[51] Constructs corresponding to domains D and E (LBD) of human RXRα fused to GST (GST-hRXRα LBD) and full-length human SRC-1a in pSG5 were kind gifts from Dr. David Heery (University of Leicester, England). GST-RXRα LBD was expressed in *E. coli* BL21(DE3)pLysS and purified by glutathione affinity chromatography using standard techniques.

Ligand Binding. hRXRα LBD was expressed in *E. coli* and purified as a polyhistidine-tagged fusion protein for use in competition binding assays.[52] Briefly, His-tagged RXR (1.0 μg) was incubated in binding buffer (0.15 M KCl in 10 mM Tris-HCl, pH 7.4, containing 0.5% 3-[(3-cholamidopropyl)dimethylammonio]-1-propane sulfonate (CHAPS detergent, Roche Diagnostics) and 8% glycerol; 300 μL) with 1 nM [11,12-$^3H_2$]9-*cis*-RA (44 Ci/mmol, NEN) in the absence or presence of increasing concentrations of nonlabeled **1** or retinoid for 16−18 h at 4 °C. Next, yttrium silicate copper His-tag beads (500 μg, Amersham Pharmacia Biotech) were added, and incubation with shaking was continued for 1 h at room temperature. The His-tagged beads were washed (3 × 1 mL of binding buffer) to separate receptor-bound from nonbound label, then suspended (500 μL of buffer) and transferred for scintillation counting (3.5 mL of EcoLume liquid scintillation fluid, ICN; Beckman Coulter LS 3801 counter). Nonspecific [^{3}H]9-*cis*-RA-binding determined in the presence of 1.0 μM nonlabeled **1** was typically less than 10% of the total bound radiolabel. Experiments were performed in duplicate, and specific binding was calculated as the average of the percentage of the total bound cpm remaining (cpm/(total bound cpm) × 100). Competitive binding using purified mRXRαΔAB and [11,12-$^3H_2$]9-*cis*-RA was conducted essentially as previously described.[51] At 1.0 μM, **1** displaced 80% ± 5% of the label from mRXRαΔAB and **3** displaced 83% ± 5%.

GST-Pulldown Experiments. Bacterially expressed GST-RXRα LBD and full-length SRC-1a, which was prepared by in vitro transcription/translation (TNT kit, Promega) in the presence of [^{35}S]methionine (NEN), were used in these studies, which were conducted as previously described.[33]

Plasmids. Expression vectors for RARα, RARβ, RARγ, and RXRα and the $(TREpal)_2$-*tk*-CAT, CRBP−I-*tk*-CAT, and CRBP−II-*tk*-CAT reporter genes were prepared as described.[53]

Receptor Transcriptional Activation in Cotransfected Cells. CV-1 cells were routinely maintained in Dulbecco's minimal essential medium (DMEM) supplemented with 10% fetal calf serum (FCS), 100 units/mL of penicillin, and 100 μg/mL of streptomycin. For transfection assays, cells were seeded at 1.0×10^5 cells/mL in 24-well plates for 16−24 h before transfection. Cells were then transfected using the calcium chloride precipitation method[54] with $(TREpal)_2$-*tk*-CAT or CRBP-I-*tk*-CAT (200 μg) alone or together with an RAR subtype vector (100 μg) or with CRBP-II-*tk*-CAT (200 μg) alone or together with RXRα (20 μg). In addition, cells were also transfected with β-galactosidase (β-gal) expression vector (pCH 110, Amersham Biosciences) and carrier DNA (pBluescript, Stratagene) to a final concentration of 1000 μg/well. At 20 h after transfection, the medium was changed to DMEM containing 5% charcoal-stripped FCS, and cells were treated for 24 h with one or more of the retinoids of interest. Chloramphenicol acetyl transferase (CAT) activity was expressed relative to β-galactosidase activity to normalize for transfection efficiency.

Western Analysis. Cell cultures were harvested and lysed in lysis buffer (50 mM Tris-HCl, pH 8.0, and 150 mM NaCl, with 0.1% Triton X-100, 0.25% sodium deoxycholate, 1 mM ethylenediaminetetraacetic acid, 1 mM phenylmethanesulfonyl fluoride, 1 μg/mL of aprotinin, 1 μg/mL of leupeptin, and 1 mM sodium orthovanadate (all from Sigma)). Equivalent protein extracts from each sample were separated on 8% SDS−PAGE gels. Protein was quantitated by a total protein assay (Bio-Rad). Proteins were transferred onto nitrocellulose membranes (Trans-Blot, Bio-Rad). Nitrocellulose membranes were preblocked with 5% nonfat milk powder in phosphate-buffered saline (PBS) containing 0.05% Tween 20 detergent for 1 h at room temperature. Following PBS/Tween washes, preblocked membranes were incubated with 1 μg/mL equivalent of anti-rabbit RARβ polyclonal antibody (Santa Cruz, CA). RARβ proteins were detected by horseradish peroxidase conjugated secondary antibodies to antirabbit immunoglobulins (Amersham Pharmacia) after a 1 h incubation at room temperature, and specific bands were visualized by enhanced chemiluminescence (ECL, Amersham Pharmacia). Equivalent loading of samples was determined by reprobing each nitrocellulose membrane with a mouse monoclonal antibody recognizing β-actin (Sigma).

Acknowledgment. We thank Dr. David Heery (University of Leicester) for the kind gifts of full-length SRC-1a and GST-RXRα LBD. These studies were supported by NIH Grants P01 CA51993 (M.I.D., M.L., and X.Z.) and P30 ES00210 (M.L.).

Supporting Information Available: Figure 7, in which the information given in Tables 1 and 2 has been expanded to other concentrations of **3** and **9** and to **2**. This material is available free of charge via the Internet at http://pubs.acs.org.

References

(1) Mangelsdorf, D. J.; Umesono, K.; Evans, R. M. The retinoid receptors. In *The Retinoids: Biology, Chemistry, and Medicine*; Sporn, M. B., Roberts, A. B., Goodman, D. S., Eds.; Raven Press: New York, 1994; pp 319−349.

(2) Bourguet, W.; Vivat, V.; Wurtz, J. M.; Chambon, P.; Gronemeyer, H.; Moras, D. Crystal structure of a heterodimeric complex of RAR and RXR ligand-binding domains. *Mol. Cell* **2000**, *5*, 289−298.

(3) Renaud, J. P.; Rochel, N.; Ruff, M.; Vivat, V.; Chambon, P.; Gronemeyer, H.; Moras, D. Crystal structure of the RARγ ligand-binding domain bound to all-trans retinoic acid. *Nature* **1995**, *378*, 681−689.

(4) Botling, J.; Castro, D. S.; Oberg, F.; Nilsson, K.; Perlmann, T. Retinoic acid receptor/retinoid X receptor heterodimers can be activated through both subunits providing a basis for synergistic transactivation and cellular differentiation. *J. Biol. Chem.* **1997**, *272*, 9443−9449.

(5) Gampe, R. T., Jr.; Montana, V. G.; Lambert, M. H.; Miller, A. B.; Bledsoe, R. K.; Milburn, M. V.; Kliewer, S. A.; Willson, T. M.; Xu, H. E. Asymmetry in the PPARγ/RXRα crystal structure reveals the molecular basis of heterodimerization among nuclear receptors. *Mol. Cell* **2000**, *5*, 545−555.

(6) Germain, P.; Iyer, J.; Zechel, C.; Gronemeyer, H. Co-regulator recruitment and the mechanism of retinoic acid receptor synergy. *Nature* **2002**, *415*, 187−192.

(7) Egea, P. F.; Mitschler, A.; Moras, D. Molecular recognition of agonist ligands by RXRs. *Mol. Endocrinol.* **2002**, *16*, 987−997.
(8) Lehmann, J. M.; Jong, L.; Fanjul, A.; Cameron, J. F.; Liu, X. P.; Haefner, P.; Dawson, M. I.; Pfahl, M. A novel class of retinoids, selective for retinoid X receptor response pathways. *Science* **1992**, *258*, 1944−1946.
(9) Dawson, M. I.; Zhang, X.; Hobbs, P. D.; Jong, L. Synthetic retinoids and their usefulness in biology and medicine. In *Vitamin A and Retinoids: An Update of Biological Aspects and Clinical Applications*; Livrea, M. A., Ed.; Birkhäuser Verlag: Basel, Switzerland, 2000; pp 161−196.
(10) Gronemeyer, H.; Miturski, R. Molecular mechanisms of retinoid action. *Cell. Mol. Biol. Lett.* **2001**, *6*, 3−52.
(11) Dawson, M. I.; Zhang, X.-K. Discovery and design of retinoic acid receptor and retinoid X receptor class- and subtype-selective synthetic analogs of all-*trans*-retinoic acid and 9-*cis*-retinoic acid. *Curr. Med. Chem.* **2002**, *9*, 623−637.
(12) Kagechika, H. Novel synthetic retinoids and separation of the pleiotropic retinoidal activities. *Curr. Med. Chem.* **2002**, *9*, 591−608.
(13) Dawson, M. I.; Jong, L.; Hobbs, P. D.; Cameron, J. F.; Chao, W. R.; Pfahl, M.; Lee, M.-O.; Shroot, B. Conformational effects on retinoid receptor selectivity. 2. Effects of retinoid bridging group on retinoid X receptor activity and selectivity. *J. Med. Chem.* **1995**, *38*, 3368−3383.
(14) Dawson, M. I.; Hobbs, P. D.; Jong, L.; Xiao, D.; Chao, W. R.; Pan, C.; Zhang, X. K. sp^2-bridged diaryl retinoids: Effects of bridge-region substitution on retinoid X receptor (RXR) selectivity. *Bioorg. Med. Chem. Lett.* **2000**, *10*, 1307−1310.
(15) Umemiya, H.; Fukasawa, H.; Ebisawa, M.; Eyrolles, L.; Kawachi, E.; Eisenmann, G.; Gronemeyer, H.; Hashimoto, Y.; Shudo, K.; Kagechika, H. Regulation of retinoidal actions by diazepinylbenzoic acids. Retinoid synergists which activate the RXR−RAR heterodimers. *J. Med. Chem.* **1997**, *40*, 4222−4234.
(16) Boehm, M. F.; Zhang, L.; Badea, B. A.; White, S. K.; Mais, D. E.; Berger, E.; Suto, C. M.; Goldman, M. E.; Heyman, R. A. Synthesis and structure−activity relationships of novel retinoid X receptor-selective retinoids. *J. Med. Chem.* **1994**, *37*, 2930−2941.
(17) Boehm, M. F.; Zhang, L.; Zhi, L.; McClurg, M. R.; Berger, E.; Wagoner, M.; Mais, D. E.; Suto, C. M.; Davies, J. A.; Heyman, R. A.; Nadzan, A. M. Design and synthesis of potent retinoid X receptor selective ligands that induce apoptosis in leukemia cells. *J. Med. Chem.* **1995**, *38*, 3146−3155.
(18) Canan Koch, S. S.; Dardashti, L. J.; Cesario, R. M.; Croston, G. E.; Boehm, M. F.; Heyman, R. A.; Nadzan, A. M. Synthesis of retinoid X receptor-specific ligands that are potent inducers of adipogenesis in 3T3-L1 cells. *J. Med. Chem.* **1999**, *42*, 742−750.
(19) Ebisawa, M.; Umemiya, H.; Ohta, K.; Fukasawa, H.; Kawachi, E.; Christoffel, G.; Gronemeyer, H.; Tsuji, M.; Hashimoto, Y.; Shudo, K.; Kagechika, H. Retinoid X receptor-antagonistic diazepinylbenzoic acids. *Chem. Pharm. Bull.* **1999**, *47*, 1778−1786.
(20) Takahashi, B.; Ohta, K.; Kawachi, E.; Fukasawa, H.; Hashimoto, Y.; Kagechika, H. Novel retinoid X receptor antagonists: Specific inhibition of retinoid synergism in RXR−RAR heterodimer actions. *J. Med. Chem.* **2002**, *45*, 3327−3330.
(21) Yamauchi, T.; Waki, H.; Kamon, J.; Murakami, K.; Motojima, K.; Komeda, K.; Miki, H.; Kubota, N.; Terauchi, Y.; Tsuchida, A.; Tsuboyama-Kasaoka, N.; Yamauchi, N.; Ide, T.; Hori, W.; Kato, S.; Fukayama, M.; Akanuma, Y.; Ezaki, O.; Itai, A.; Nagai, R.; Kimura, S.; Tobe, K.; Kagechika, H.; Shudo, K.; Kadowaki, T. Inhibition of RXR and PPARγ ameliorates diet-induced obesity and type 2 diabetes. *J. Clin. Invest.* **2001**, *108*, 1001−1013.
(22) Canan Koch, S. S.; Dardashti, L. J.; Hebert, J. J.; White, S. K.; Croston, G. E.; Flatten, K. S.; Heyman, R. A.; Nadzan, A. M. Identification of the first retinoid X receptor homodimer antagonist. *J. Med. Chem.* **1996**, *39*, 3229−3234.
(23) Cavasotto, C. N.; Orry, A. J.; Abagyan, R. A. Structure-based identification of binding sites, native ligands and potential inhibitors for G-protein coupled receptors. *Proteins* **2003**, *51*, 423−433.
(24) Cavasotto, C. N.; Abagyan, R. A. Protein flexibility in ligand docking and virtual screening to protein kinases. *J. Mol. Biol.* **2004**, *337*, 209−225.
(25) Vivat, V.; Zechel, C.; Wurtz, J. M.; Bourguet, W.; Kagechika, H.; Umemiya, H.; Shudo, K.; Moras, D.; Gronemeyer, H.; Chambon, P. A mutation mimicking ligand-induced conformational change yields a constitutive RXR that senses allosteric effects in heterodimers. *EMBO J.* **1997**, *16*, 5697−5709.
(26) Apfel, C.; Bauer, F.; Crettaz, M.; Forni, L.; Kamber, M.; Kaufmann, F.; LeMotte, P.; Pirson, W.; Klaus, M. A retinoic acid receptor α antagonist selectively counteracts retinoic acid effects. *Proc. Natl. Acad. Sci. U.S.A.* **1992**, *89*, 7129−7133.
(27) Lee, M.-O.; Hobbs, P. D.; Zhang, X.-K.; Dawson, M. I.; Pfahl, M. A synthetic retinoid antagonist inhibits the human immunodeficiency virus type 1 promoter. *Proc. Natl. Acad. Sci. U.S.A.* **1994**, *91*, 5632−5636.
(28) Lipinski, C. A.; Lombardo, F.; Dominy, B. W.; Feeney, P. J. Experimental and computational approaches to estimate solubility and permeability in drug discovery and development settings. *Adv. Drug Delivery Rev.* **2001**, *46*, 3−26.
(29) Xu, X. C.; Sozzi, G.; Lee, J. S.; Lee, J. J.; Pastorino, U.; Pilotti, S.; Kurie, J. M.; Hong, W. K.; Lotan, R. Suppression of retinoic acid receptor β in non-small-cell lung cancer in vivo: Implications for lung cancer development. *J. Natl. Cancer Inst.* **1997**, *89*, 624−629.
(30) Xu, X. C.; Sneige, N.; Liu, X.; Nandagiri, R.; Lee, J. J.; Lukmanji, F.; Hortobagyi, G.; Lippman, S. M.; Dhingra, K.; Lotan, R. Progressive decrease in nuclear retinoic acid receptor β messenger RNA level during breast carcinogenesis. *Cancer Res.* **1997**, *57*, 4992−4996.
(31) Li, X.-S.; Shao, Z.-M.; Sheikh, M. S.; Eiseman, J. L.; Sentz, D.; Jetten, A. M.; Chen, J.-C.; Dawson, M. I.; Aisner, S.; Rishi, A. K.; Fontana, J. A. Retinoic acid nuclear receptor β (RARβ) inhibits breast carcinoma anchorage independent growth. *J. Cell. Physiol.* **1995**, *165*, 449−458.
(32) Liu, Y.; Lee, M.-O.; Wang, H.-G.; Li, Y.; Hashimoto, Y.; Klaus, M.; Reed, J. C.; Zhang, X. RARβ mediates the growth-inhibitory effect of retinoic acid by promoting apoptosis in human breast cancer cells. *Mol. Cell. Biol.* **1996**, *16*, 1138−1149.
(33) James, S. Y.; Lin, F.; Kolluri, S. K.; Dawson, M. I.; Zhang, X.-K. Regulation of retinoic acid receptor β expression by peroxisome proliferator-activated receptor γ ligands in cancer cells. *Cancer Res.* **2003**, *63*, 3531−3538.
(34) Peterson, V. J.; Barofsky, E.; Deinzer, M. L.; Dawson, M. I.; Feng, K.-C.; Zhang, X.-K.; Madduru, M. R.; Leid, M. Mass-spectrometric analysis of agonist-induced retinoic acid receptor γ conformational change. *Biochem. J.* **2002**, *362*, 173−181.
(35) Egea, P. F.; Mitschler, A.; Rochel, N.; Ruff, M.; Chambon, P.; Moras, D. Crystal structure of the human RXRα ligand-binding domain bound to its natural ligand: 9-*cis*-retinoic acid. *EMBO J.* **2000**, *19*, 2592−2601.
(36) *ICM Manual*, 3rd ed.; Molsoft L.L.C.: La Jolla, CA, 2003.
(37) Love, J. D.; Gooch, J. T.; Benko, S.; Li, C.; Nagy, L.; Chatterjee, V. K.; Evans, R. M.; Schwabe, J. W. The structural basis for the specificity of retinoid-X receptor-selective agonists: New insights into the role of helix H12. *J. Biol. Chem.* **2002**, *277*, 11385−11391.
(38) Sakashita, A.; Kizaki, M.; Pakkala, S.; Schiller, G.; Tsuruoka, N.; Tomosaki, R.; Cameron, J. F.; Dawson, M. I.; Koeffler, H. P. 9-*cis*-Retinoic acid: Effects on normal and leukemic hematopoiesis in vitro. *Blood* **1993**, *81*, 1009−1016.
(39) Dawson, M. I.; Chan, R. L.-S.; Derdzinski, K.; Hobbs, P. D.; Chao, W.-R.; Schiff, L. J. Synthesis and pharmacological activity of 6-[(*E*)-2-(2,6,6-trimethyl-1-cyclohexen-1-yl)ethen-1-yl]- and 6-(1,2,3,4-tetrahydro-1,1,4,4-tetramethyl-6-naphthyl)-2-naphthalenecarboxylic acids. *J. Med. Chem.* **1983**, *26*, 1653−1656.
(40) Faul, M. M.; Ratz, A. M.; Sullivan, K. A.; Trankle, W. G.; Winneroski, L. L. Synthesis of novel retinoid X receptor-selective retinoids. *J. Org. Chem.* **2001**, *66*, 5772−5782.
(41) Abagyan, R.; Totrov, M. Biased probability Monte-Carlo conformational searches and electrostatic calculations for peptides and proteins. *J. Mol. Biol.* **1994**, *235*, 983−1002.
(42) Abagyan, R.; Totrov, M.; Kuznetsov, D. ICM—A new method for protein modeling and design—Applications to docking and structure prediction from the distorted native conformation. *J. Comput. Chem.* **1994**, *15*, 488−506.
(43) Némethy, G.; Gibson, K. D.; Palmer, K. A.; Yoon, C. N.; Paterlini, G.; Zagari, A.; Rumsey, S.; Scheraga, H. A. Energy parameters in polypeptides. 10. Improved geometrical parameters and nonbonded interactions for use in the ECEPP/3 algorithm, with application to proline-containing peptides. *J. Phys. Chem.* **1992**, *96*, 6472−6484.
(44) Abagyan, R. A.; Totrov, M. Ab initio folding of peptides by the optimal-bias Monte Carlo minimization procedure. *J. Comput. Phys.* **1999**, *151*, 402−421.
(45) Metropolis, N.; Rosenbluth, A. W.; Rosenbluth, M. N.; Teller, A. H.; Teller, E. Equation of state calculations by fast computing machines. *J. Chem. Phys.* **1953**, *21*, 1087−1092.
(46) Totrov, M.; Abagyan, R. The contour-buildup algorithm to calculate the analytical molecular surface. *J. Struct. Biol.* **1996**, *116*, 138−143.
(47) Totrov, M.; Abagyan, R. Protein−ligand docking as an energy optimization problem. In *Drug−Receptor Thermodynamics: In-*

troduction and Experimental Applications; Raffa, R. B., Ed.; John Wiley and Sons: New York, 2001; pp 603−624.
(48) Totrov, M.; Abagyan, R. Derivation of the sensitive discrimination potential for virtual ligand screening. In *RECOMB '99: Proceedings of the Third Annual International Conference on Computational Molecular Biology*; Waterman, M., Ed.; Association for Computer Machinery, New York: Lyon, France, 1999; pp 37−38.
(49) Totrov, M.; Abagyan, R. Flexible protein−ligand docking by global energy optimization in internal coordinates. *Proteins* **1997**, Suppl. 1, 215−220.
(50) Schapira, M.; Totrov, M.; Abagyan, R. Prediction of the binding energy for small molecules, peptides and proteins. *J. Mol. Recognit.* **1999**, *12*, 177−190.
(51) Leid, M. Ligand-induced alteration of the protease sensitivity of retinoid X receptor α. *J. Biol. Chem.* **1994**, *269*, 14175−14181.
(52) Allegretto, E. A. Detection of RARs and RXRs in cells and tissues using specific ligand-binding assays and ligand-binding immunoprecipitation techniques. In *Methods in Molecular Biology: Retinoid Protocols*; Redfern, C. P. F., Ed.; Humana Press: Totowa, NJ, 1998; pp 219−232.
(53) Zhang, X.-K.; Hoffmann, B.; Tran, P. B.; Graupner, G.; Pfahl, M. Retinoid X receptor is an auxiliary protein for thyroid hormone and retinoic acid receptors. *Nature* **1992**, *355*, 441−446.
(54) Wu, Q.; Dawson, M. I.; Zheng, Y.; Hobbs, P. D.; Agadir, A.; Jong, L.; Li, Y.; Liu, R.; Lin, B.; Zhang, X.-K. Inhibition of *trans*-retinoic acid-resistant human breast cancer cell growth by retinoid X receptor-selective retinoids. *Mol. Cell. Biol.* **1997**, *17*, 6598−6608.

JM030651G